# Modelling of the JET current ramp up experiments and projection to ITER

I. Voitsekhovitch[1], A. C. C. Sips[2], B. Alper[1], M. Beurskens[1], I. Coffey[1], J. Conboy[1], T. Gerbaud[3], C. Giroud[1], T. Johnson[4], F. Köchl[5], E. de la Luna[1], D. C. McDonald[1], I. Pavlenko[6], G. V. Pereverzev[7], S. Popovichev[1], G. Sergienko[8], S. Sharapov[1], M. Stamp[1] and JET-EFDA contributors*

*JET-EFDA, Culham Science Centre, Abingdon, Oxon, OX14 3DB, UK*

*[1]EURATOM/CCFE Association, Culham Science Centre, Abingdon, Oxon, OX14 3DB, UK*

*[2]European Commission, B-1099, Brussels, Belgium*

*[3]Association Euratom CEA, CEA/DSM/IRFM, Cadarache, 13108 Saint-Paul-lez-Durance, France*

*[4]Association EURATOM-VR, KTH Stockholm, Sweden*

*[5]Association EURATOM-AW/ATI, Vienna, Austria*

*[6]Dept. of Physics and Technology, Kharkiv National University, Ukraine*

*[7]Max-Planck Institut für Plasmaphysik, IPP-Euratom Association, D-85748 Garching bei München, Germany*

*[8]Institut für Energieforschung IEF-4 (Plasmaphysik), Forschungszentrum Jülich GmbH, EURATOM Association, Trilateral Euregio Cluster (TEC), D-52425 Jülich, Germany*

See appendix of F. Romanelli et al., IAEA Fusion Energy Conference 2008 (Proc. 22nd Int. Conf. Geneva 2008) IAEA Vienna (2008)

**Abstract**

The current ramp up phase of ITER demonstration discharges, performed at JET, is analysed and the capability of the empirical *L*-mode Bohm-gyroBohm and Coppi-Tang transport models as well as the theory-based GLF23 model to predict the temperature evolution in these discharges is examined. The analysed database includes ohmic (OH) plasmas with various current ramp rates and plasma densities and the *L*-mode plasmas with the ion cyclotron radio frequency (ICRF) and neutral beam injection (NBI) heating performed at various ICRF resonance positions and NBI heating powers. The emphasis of this analysis is a data consistency test, which is particularly important here because some parameters, useful for the transport model validation, are not measured in OH and ICRF heated plasmas (e.g. ion temperature, effective charge). The sensitivity of the predictive accuracy of the transport models to the unmeasured data is estimated. It is found that the Bohm-gyroBohm model satisfactorily predicts the temperature evolution in discharges with central heating (the *rms* deviation between the simulated and measured temperature is within 15%), but underestimates the thermal electron transport in the OH and off-axis ICRF heated discharges. The Coppi-Tang model strongly underestimates the thermal transport in all discharges considered. A re-normalisation of these empirical models for improving their predictive capability is proposed. The GLF23 model, strongly dependent on the ion temperature gradient and tested only for NBI heated discharges with measured ion temperatures, predicts accurately the temperature in the low power NBI heated discharge (*rms* < 10%) while the discrepancy with the data increases at high power. Based on the analysis of the JET discharges, the modelling of the current ramp up phase for the H-mode ITER scenario is performed with particular emphasis on the

sensitivity of the duration of the sawtooth-free current ramp up phase to transport model.

## I. Introduction

The current ramp up phase in tokamaks has recently attracted the attention of experimentalists [1-3] and modellers [1, 4 - 6] in connection with future experiments on ITER. The important objectives of the current ramp up phase on ITER are maintenance of a current density profile compatible with vertical stability of the plasma column [7] and the formation of the target $q$-profile favourable for subsequent burn phase (with $q_0$ above one for an extended sawtooth-free H-mode and Hybrid scenario or reversed $q$ profile for the advanced operation with an internal transport barrier (ITB)) [8]. Keeping in mind these objectives the effects of various parameters, such as the current ramp rate [3], plasma density [3], additional heating [2, 3] and variation of the plasma shape and volume [1] on the optimisation of the current ramp up phase have been investigated. The current profile diffusion is a key issue of this study. Since the current diffusion is strongly affected by the evolution of electron temperature, the analysis of the thermal electron transport in present current ramp up experiments and the identification of the transport model for thermal electron transport becomes essential for understanding the physics processes occurring during the current ramp up, more reliable predictions and optimisation of this phase in future experiments.

The modelling of the current ramp up scenarios performed up to now includes both the validation of the transport models against the existing experiments and their application to ITER. Thus, the electron temperature in the DIII-D current ramp up discharges described above [1] has been accurately simulated with the Coppi-Tang model [9] and this model has been used later on for the examination of the plasma operating space for the ITER 15 MA ELMy H-mode inductive scenario (poloidal field

capability and divertor design [4]). At JET the temperature evolution during the Ohmic (OH) and auxiliary heated (lower hybrid current drive (LHCD) and ion cyclotron radio frequency (ICRF) heating) current ramp up phase of scenarios with an ITB, has been successfully simulated using the empirical Bohm-gyroBohm type of the transport model [10, 11] together with a simple ETG-like thermal electron transport coefficient [12]. Later on the validation of the Bohm-gyroBohm model [10] has been performed also for ohmic and LHCD assisted current ramp up phase of the H-mode discharges of JET [6]. Finally, the empirical formula for the thermal electron diffusivity which has a parabolic profile multiplied by a free coefficient adjusted at each time step to provide a prescribed $H_{98y}$ factor has been validated against the OH current ramp up discharges of JET, performed at two different current ramp rates, and applied to the modelling of the ITER ramp up phase [5].

In this work the current ramp up phase of the ITER demonstration discharges performed at JET [3] is analysed and used for the estimation of the predictive accuracy of various thermal transport models. The selected database includes the discharges representing single parameter scans: the OH discharges performed at three different current ramp rates with other operational parameters kept similar, the OH discharges with varied electron density and the auxiliary heated current ramp up. The latter group of discharges includes on-axis and off-axis ICRF heating with 3 MW of applied power and the NBI heating performed with different power. The interpretative analysis of these discharges is carried out here by using the TRANSP code [13]. Since the OH and ICRF heated plasmas are poorly diagnosed this analysis has been focused on the data consistency and estimation of the constraints on the non-measured quantities such as ion temperature $T_i$ and the profile of the effective charge $Z_{eff}$. The

determined range of the non-measured quantities has been used for the estimation of the sensitivity of the predictive accuracy of the transport models to these parameters.

Three transport models – the empirical L-mode Bohm-gyroBohm model with the electron pressure gradient driven transport [11], the theory-based GLF23 model which includes the ion temperature gradient (ITG), electron temperature gradient (ETG) and trapped electron mode (TEM) driven transport [14] and the empirical Coppi-Tang model based on the principle of profile consistency and coupling the thermal transport with the plasma geometry and density [9] – have been tested. Since two of the selected empirical models (Bohm-gyroBohm and Coppi-Tang) do not include a dependence on the ion temperature, they have been tested for all considered discharges including the OH and ICRF heated pulses. The GLF23 model, strongly dependent on the ion temperature gradient, has been tested only for the NBI heated current ramp up scenario where the measurements of $T_i$ are available. Summarising briefly the modelling results, a satisfactory predictive accuracy of the Bohm-gyroBohm model with the *rms* deviation between the simulated and measured temperature less than 15% has been found in the discharges with central heating while this model overestimates the electron temperature in the OH and off-axis ICRF heated discharge (the *rms* deviation increases up to 46%). The GLF23 model predicts temperatures rather accurately at low NBI power (within 10% of the *rms* deviation), but its predictive accuracy reduces with power (*rms* increases up to 28.17% at 9.8 MW). The Bohm-gyroBohm and GLF23 model have been tested for the restricted plasma region $0 \leq \rho \leq 0.85$ (here $\rho = \Phi^{0.5}$, $\Phi$ is the toroidal flux) because of the poor electron density measurements near the plasma edge after the breakdown. The Coppi-Tang model, weakly sensitive to the uncertainty in the edge density, has been tested

for the whole plasma region providing a relatively accurate temperature prediction near the edge, but strongly overestimating the core temperature in all discharges.

Based on the results obtained with the empirical models the possibility of the re-normalisation of these models for improving their predictive accuracy in the regimes where it is unsatisfactory has been examined. The multiplication factor for the Bohm-gyroBohm and Coppi-Tang thermal electron and ion diffusivities minimising the *rms* deviation within each group of discharges characterised by different heating methods (OH, ICRH and NBI) has been determined. With this re-normalisation the *rms* deviation for electron temperature has been reduced below 11.4% in the simulations with the Bohm-gyroBohm model performed for all OH discharges and the pulse with the off-axis ICRF heating. The predictive accuracy of the re-normalised Coppi-Tang model improves as well resulting in *rms* deviations in the range 6.2 - 31.2%. The sensitivity of the artificial multipliers in empirical transport coefficients to the uncertainties in the measured plasma parameters will be discussed.

After performing the model validation against the JET discharges the original Bohm-gyroBohm and GLF23 models have been used in the predictive simulations of the current ramp up in ITER. The goal of these simulations is the estimation of the sawtooth-free current ramp up phase under different assumptions on the transport model, when ramping the plasma current to 15 MA in 80 s in plasmas with 2 – 20 MW of central electron heating (the baseline H-mode ITER scenario is considered here). A clear difference in the duration of the phase with $q_0 > 1$ has been obtained in the simulations with different transport models at all heating powers (up to 19 s, with a longer duration obtained with the GLF23 model). The central electron heating extends the duration of this phase from 17.5 to 34 s in simulations with the Bohm-

gyroBohm model and from 31.5 to 50.5 s in simulations with the GLF23 model when the electron heating power increases from 2 to 20 MW. A broader sawtooth mixing region forms at the end of the current ramp up in the simulations with the Bohm-gyroBohm model under assumption of the Kadomtsev reconnection mechanism. These differences in the current diffusion are caused by the different transient electron temperature evolution at the beginning of the central electron heating with the GLF23 model predicting a higher temperature and broader $T_e$ profile. At the end of the current ramp up similar central temperatures are predicted with the two models at low heating power (less than 8 MW) with a slightly more peaked $T_e$ profile obtained with the GLF23 model. The difference in the predicted central temperature increases with power reaching 22% at 20 MW with a larger temperature (8.3 keV) obtained in simulations with the Bohm-gyroBohm model. Finally, a non-monotonic dependence of the duration of the phase with $q_0 > 1$ on the electron heating power has been found in simulations with the Bohm-gyroBohm model which may be useful for the scenario optimisation.

This paper is organised as follows. The selected JET discharges are briefly described in Section II. Section III is dedicated to the analysis of these discharges, tests of data consistency and estimation of the constraints on the non-measured quantities affecting transport and current diffusion. The effect of the density, current ramp rate and plasma heating on the $q$-profile evolution in JET discharges is described in Section IV. The validation of the transport models is presented in Section V. The modelling of the current ramp up phase in ITER is shown in Section VI. Finally, the results of this paper are summarised and discussed in Section VII.

## II. Experimental database

The current ramp up experiments analysed here have been performed at 2.4 T in deuterium plasmas with low triangularity ($\delta_u$ = 0.14 – 0.17, $\delta_l$ = 0.24 - 0.28). The plasma current has been raised to 2.7 MA in all discharges considered, i.e. $q_{95}$ = 3 has been achieved at the current flat-top. The plasma has been expanded till full volume very early in the discharge. Three types of the scenarios including the OH, ICRF and NBI heated current ramp up have been analysed (Figs. 1 - 3 and tables 1 and 2).

The ohmic discharges have been performed with three different current ramp rates $dI_{pl}/dt$ varying from shot to shot (#72464, 72465 and 72467 in table 1 and Fig. 1, top panel). These three discharges are characterised by a similar evolution of the central line averaged density $n_l$ increasing with plasma current (Fig. 1, middle panel). The evolution of the central electron temperature is also similar in these discharges, while the temperature at mid-radius increases faster at a faster current ramp up (Fig. 1, bottom panel). The sawtooth crashes have been observed after 5.5 – 6 s in discharges with moderate (0.28 MA/s) and slow (0.19 MA/s) current ramp-up, limiting the core electron temperature. At high current ramp rate ($dI_{pl}/dt$ = 0.36 MA/s, #72464) the current ramp-up phase was sawtooth-free.

The discharges with fast (#72460 and #72464) and medium (#72467, 72504 and 72723) current ramp rate have been performed with electron density varied from shot to shot by changing the deuterium gas puff. The effective charge of plasma increases as the plasma density reduces, but this reduction saturates at low density (#72460 and #72464 have nearly the same $Z_{eff}$). The NBI heating applied at the end of the current ramp up in these and the ICRH heated discharges causes a rapid increase of the electron density, but the main NBI heating phase performed during the plasma current plateau is excluded from our analysis.

One of the OH discharges (#72467) has been used as a reference for the study of the effect of the ICRF heating on the current ramp up. The on-axis and off-axis hydrogen minority heating with 3 MW of injected power in plasmas with 6 - 7% of hydrogen concentration (Fig. 2, top panel) has been performed by applying the antenna frequency of 37 (#72507) and 47 (#72505) MHz correspondingly (the ICRF resonance position was around 2.97 and 2.36 m respectively). The ICRF heated discharges and reference OH discharge show similar density evolution (Fig. 2, middle panel), but $Z_{eff}$ is larger in discharges with the ICRF heating ($Z_{eff}$ = 2.6 in #72507 and $Z_{eff}$ = 3 in #72505). Larger central electron temperature has been achieved in discharges with central heating (Fig. 2, bottom panel). The first sawtooth crash is observed much later in this discharge (at 7.46 s) as compared to the reference OH discharge (before 6 s) while the discharge with the off-axis heating has early frequent small-amplitude sawtooth oscillations.

The NBI heated discharges have been performed with three different powers varying from 4 to 9.8 MW and similar electron density and $Z_{eff}$ (table 2 and Fig. 3). The confinement regime changes with power in these discharges passing from the *L*-mode confinement during the whole ramp up phase at 4 MW of NBI heating (#72516) to the *H*-mode confinement achieved around 7 s in the discharge with medium power (#72511) and around 5.16 s in the discharge with high power (#72512). Transient steep ITB-like ion temperature profiles have been observed in #72512 after 5 s. The electron and ion temperature are similar in the *L*-mode plasmas at low NBI power, while $T_i > T_e$ at high power where the NBI ion heating is dominant (Fig. 3, bottom panel). Sawtooth oscillations have been observed after 6.58 s in the low power discharge (#72516). In two other discharges no sawtooth crashes have been observed during the current ramp-up. Although the *L-H* transition occurred in two NBI heated

discharges during the current ramp-up the transport analysis performed here will be focused on their *L*-mode phase.

The data from the following diagnostics have been used for this study. The electron temperature has been measured using an ECE diagnostic with a spatial resolution of about 5 cm and time resolution of 22 ms, and a Thomson scattering diagnostic with a spatial resolution of 5 cm and time resolution of 250 ms. The same Thomson scattering diagnostic has been used for the measurements of electron density. A 12 channel charge-exchange (CX) diagnostic with a 10 ms time resolution has been used for the measurements of ion temperature, toroidal rotation of carbon impurity and effective charge of plasma in the outer half of plasma column in the NBI heated discharges. Bolometer measurements have been used for the bulk radiation, and the radiative power profiles have been reconstructed for few discharges using 10 diagnostic channels covering the upper half of plasma column. The neutron yield from the 2.5 MeV neutrons measured by three toroidally separated detectors, the diamagnetic energy obtained in the EFIT [15] simulations constrained by the magnetic probe measurements, and the measured soft X-ray emission have been used for the data consistency analysis. In the OH and ICRF heated scenarios where the CX measurements of $Z_{eff}$ profile are not available the bremsstrahlung measurements of vertical line averaged $Z_{eff}$ have been used. The typical error bars of the bremsstrahlung measurements of $Z_{eff}$ are around 20%.

## III. Data consistency analysis

In the experiments considered, the current ramp-up phase is not always sufficiently diagnosed. In particular, some parameters, important for the transport

model validation such as $Z_{eff}$ profile, ion temperature and toroidal rotation velocity are not measured in the OH and ICRF heated plasmas. The MSE measurements providing a more accurate reconstruction of $q$-profile are not available for analysed discharges. In the NBI heated discharges the measurements of $Z_{eff}$ profile are limited to carbon impurities only.

In the absence of all required quantities being measured, a data consistency test has been used for the approximate estimation of the non-measured parameters. The data consistency analysis performed here includes the simulations of the neutron yield $R_n$, diamagnetic energy $W_{dia}$ and current density profile using the available measurements and various assumptions on the unknown ion temperature and $Z_{eff}$. As a result, the ion temperature and $Z_{eff}$ profiles matching the measured $R_n$, $W_{dia}$ and the evolution of the central safety factor $q_0$ consistent with the time of the first sawtooth crash $t_{saw}$ indicated by the soft X-ray emission have been determined. The restriction on the central safety factor has been eased by allowing $q_0(t_{saw}) = 0.7 - 1$. Here the adjustment procedure has been performed manually; the development of an automatic procedure for the estimation of the non-measured quantities with uncertainties, consistent with various measured global parameters is in progress [16, 17]. It should be mentioned that the data consistency test does not give a unique solution for the unknown quantities. Instead it allows one to estimate the possible range for these quantities. That is why the subsequent analysis will be completed with a sensitivity study illustrating the effect of the variation of the constrained non-measured parameters on the predictive accuracy of various transport models.

The TRANSP code [13] is the main simulation tool used here for the data consistency test. Taking the plasma boundary reconstructed by EFIT, TRANSP simulates the plasma equilibrium, solves the poloidal field diffusion equation and

calculates the heating and current drive (for NBI heated discharges) sources, fast ion pressure (for ICRF and NBI heated plasmas), neutron yield and diamagnetic energy. The current profile diffusion is simulated in TRANSP using the neoclassical current conductivity and the bootstrap current determined by NCLASS [18].

### *a) ohmic current ramp up*

In this section the data consistency analysis is described in detail, taking the low density OH discharge (#72460) as an example. A similar analysis has been performed for other ohmic discharges.

The first step of this analysis is the simulation of the current diffusion in OH plasmas. The current density is generally sensitive to the electron temperature and $Z_{eff}$ profile which affect the current penetration and final stationary current density profile due to the temperature and $Z_{eff}$ dependent current conductivity $\sigma \sim T_e^{3/2}/Z_{eff}$. A higher electron temperature delays the current penetration and a broader $T_e$ profile leads to the formation of a broader stationary current density profile with a higher $q_0$ in plasmas with the dominant OH current (an illustration of the influence of the $T_e$ peaking on the stationary current density profiles in JET discharges is given in Ref. 19). The effective charge affects the current density evolution in two opposite ways: the current penetration is faster in impure plasmas leading to a reduction of the core safety factor, but a broader stationary current density profile forms with centrally peaked impurity concentration increasing the core safety factor. Because of the complicated interplay between these two effects working in opposite directions it is difficult to predict analytically the dominant effect of $Z_{eff}$ on the current density profile for each particular case.

The comparison of the electron temperature profiles obtained with the ECE diagnostics and profiles obtained after a slight smoothing of the Thomson scattering data shows that the ECE $T_e$ profiles are generally more peaked. By estimating the $T_e$ peaking factor as the ratio of the temperatures measured at 3 and 3.5 m averaged over the ramp up phase it was found that the peaking of the electron temperature obtained with the ECE data is 13 - 19% larger than the peaking factor obtained with the Thomson scattering data.

The effect of the peaking of electron temperature on the $q$-profile evolution is illustrated in Fig. 4 (top panel) showing the central safety factor simulated by TRANSP using the ECE (red solid curve) and Thomson scattering data (red dashed curve) for $T_e$ and flat $Z_{eff}$ profile (the simplest starting assumption). The reduction of $q_0$ is strongly delayed with a broader $T_e$ profile, the $q_0$ value at the time of the first sawtooth crash ($t_{saw}$ = 6.9 s) obtained in simulations with Thomson scattering and ECE data is equal to 0.72 and 0.56 correspondingly. The $q_0$ simulated with the Thomson scattering data for $T_e$ may be still consistent with the measured time of the first sawtooth crash, but the $q_0$ based on the ECE data is too low. For five other discharges the $q_0$ obtained with the Thomson scattering and ECE data for $T_e$ reduces to 0.59 - 0.67 and 0.5 - 0.56 correspondingly by the time of the first sawtooth crash.

As a next step, the sensitivity of the $q_0$ evolution to $Z_{eff}$ peaking has been tested by assuming a profile of carbon impurity $n_C \propto (1 - (\rho - \rho_0)^2)^\gamma$ (with $\rho_0 = 0$ for OH discharges) and varying the exponent $\gamma$ while keeping the prescribed (measured) line averaged $Z_{eff}$. The ECE data for $T_e$ requiring larger modification of $Z_{eff}$ have been used in these simulations. The adjustment of the impurity peaking has been performed with the ASTRA [20] code due to its larger input flexibility. Before doing this adjustment, the simulations of the current diffusion with ASTRA and TRANSP have been

compared by using the TRANSP output parameters (density, $T_e$, flat $Z_{eff}$, etc.) as an input to ASTRA. Good agreement between these two codes has been obtained (solid blue and red curves in Fig. 4, top panel). Then, by adjusting the impurity profile peaking in ASTRA simulations of current diffusion the $q$ profile evolution with $q_0(t_{saw}) = 0.8$ has been obtained (blue dashed curve in Fig. 4, top panel). The profile of effective charge and deuterium density corresponding to this case are shown in the middle and bottom panel of Fig. 4.

The simulations described above have been performed assuming equal electron and ion temperature. The current diffusion in plasmas with low bootstrap current fractions is weakly sensitive to the assumption on $T_i$. As a next step in the data consistency test, the ion temperature has been determined assuming that $T_i$ profile is similar to $T_e$ profile and adjusting the $T_i/T_e$ ratio in the TRANSP simulations of the neutron yield until the measured neutron yield is matched. Although the neutron statistics are relatively low in the OH plasmas, the data from three toroidally separated neutron detectors are in a good agreement for all OH discharges suggesting that the measured neutron yield, highly sensitive to the ion temperature, can be used for the rough estimation of $T_i$. The neutron yield has been strongly overestimated in simulations with both flat and peaked $Z_{eff}$ profiles (Fig. 4, middle panel) and $T_i/T_e = 1$ for discharge 72460 (Fig. 5, red curves). By reducing the $T_i/T_e$ ratio from 1 to 0.88 for the first 2.5 s of the current ramp up and further to 0.81 after 3.7 s a more accurate prediction of neutron emission has been obtained (Fig. 5, blue curve). For the other five discharges performed at higher density a good agreement between the simulated and measured neutron yield has been obtained under assumption of $T_i/T_e = 1$ in simulations with the ECE data for $T_e$ and centrally peaked $Z_{eff}$ profile providing the $q_0$ evolution consistent with the time of the first sawtooth crash.

### *b) ICRF assisted current ramp up*

Similar adjustment of $Z_{eff}$ and ion temperature has been performed for two ICRF heated discharges. The ohmic current, simulated with a flat $Z_{eff}$ profiles, penetrates rapidly towards the centre in these discharges leading to a fast reduction of $q_0$ ($q_0$ = 0.63 - 0.69 at $t_{saw}$ = 4.5 s in #72505 and $q_0$ = 0.5 – 0.6 at $t_{saw}$ = 7.47 s in #72507. Here the range of $q_0$ is determined by the ECE and Thomson scattering data for $T_e$). Similar to the OH plasmas the neutron yield is strongly overestimated under the assumptions of $T_i = T_e$ and flat $Z_{eff}$ profile matching its measured line averaged value. An attempt to increase the $q_0(t_{saw})$ by varying the carbon impurity profile has been performed in simulations with the ECE data for electron temperature using TRANSP and ASTRA codes. Since the ICRF heated discharges have relatively high impurity content ($Z_{eff}$ = 2.6 - 3) and low electron density the central impurity peaking was limited by the quasi-neutrality of the core plasma that does not allow to obtain a sufficient delay of the $q_0$. Another solution for maintaining the simulated $q_0$ above 0.7 till the first sawtooth crash has been found by using the parabolic off-axis carbon impurity profile resulting in the off-axis $Z_{eff}$ profile with its maximum value of 4.5 - 5.5 for #72505, and 5 - 6.5 for #72507, located at $\rho_0$ = 0.8 - 0.9. The current density evolution obtained with this $Z_{eff}$ profile will be discussed in Section IV. Finally, the ion to electron temperature ratio matching the measured neutron yield in simulations with the off-axis $Z_{eff}$ profile is around 0.6.

### *c) NBI assisted current ramp up*

In the NBI heated discharges the CX diagnostic beam has been used for the measurements of ion temperature, carbon concentration and toroidal rotation velocity.

The measured $Z_{eff}$ profile is nearly flat or slightly off-axis in these discharges and its shape weakly varies during the current ramp up (Fig. 6). The neutron yield simulated by TRANSP with the measured $T_i$ and $Z_{eff}$ is overestimated by about 30% as compared to measurements in the analysed NBI heated discharges. Taking a low power NBI heated discharge as an example and adding a heavier impurity, for example, iron (the VUV survey spectrometer monitoring the plasma impurity shows a high concentration of iron in the these discharges), the agreement between the simulated and measured neutron yield can be achieved by adjusting the peaking of the Fe impurity profile. However, the core $Z_{eff}$ will be unrealistically high in this case ($Z_{eff}(\rho = 0) \geq 15$). Other factors affecting the simulated neutron yield could be the anomalous losses of fast ions and CX losses of fast neutrals. The anomalous fast ion losses are not considered here because of the absence of the measurements proving such losses in the analysed discharges. The sensitivity of the neutron yield to the CX losses of injected fast neutrals has been estimated under the assumption of zero recycling of fast neutrals by varying the wall neutral concentration in TRANSP simulations for discharge 72516. A good agreement with the measured neutron yield has been achieved with the edge density of wall neutrals varying during the current ramp up in the range $(0.5 - 2)10^{11}$ $m^{-3}$. However, the CX power losses are quite significant in this case reaching 32%. The obtained concentration of the neutral density also needs to be confirmed by measurements.

Similar to the OH and ICRF heated plasmas the current diffusion simulated using the measured $Z_{eff}$ profile and ECE data for electron temperature occurs too rapidly in the NBI heated discharges 72516 and 72511 leading to $q_0(t_{saw}) = 0.55 – 0.58$. A larger $q_0$ at the time of the first sawtooth crash is obtained with the broader $T_e$ profiles measured with the Thomson scattering diagnostics ($q_0 = 0.67$ at $t_{saw} = 6.58$ s

in #72516 and $q_0$ > 0.7 till the end of the current ramp up in #72511). The $q_0$ simulated with the ECE and Thomson scattering data for #72512 reduces to 0.87 and 1.19 correspondingly by the end of the current ramp up. The soft X-ray data show no sawtooth oscillations during the current ramp up phase in this discharge.

Summarising the results of the data consistency analysis, the range of $Z_{eff}$ profiles varying from flat (simplest assumption) to peaked (providing a reasonable $q_0$ value at the time of the first sawtooth crash), and the range of the ion to electron temperature ratio varying from 1 down to smaller values, matching the measured neutron yield, have been taken into account in the estimation of the predictive accuracy of the transport models for ohmic and ICRF heated discharges. For the NBI heated discharges the dataset, which includes the measured carbon impurity concentration, toroidal rotation velocity and ion temperature, has been used for the transport model validation. Since the Thomson scattering data are noisy the ECE measurements of electron temperature will be used for the estimation of the predictive accuracy of the transport models, but the comparison of the simulated $T_e$ with the Thomson scattering measurements will be shown as well.

## IV. Current profile diffusion in OH and auxiliary heated discharges

Here the effects of the current ramp rate, plasma density and auxiliary heating on the current profile diffusion simulated with $Z_{eff}$ profile and $T_i/T_e$ ratio determined in the previous section are briefly summarised.

The evolution of the current density and temperature in OH discharges with slow (#72465, $dI_{pl}/dt$ = 0.19 MA/s) and fast ($dI_{pl}/dt$ =0.36 MA/s, #72464) current

ramp up is shown in Fig. 7. The current diffusion in these discharges has been simulated with TRANSP starting from 2.05 s when the data quality is reasonably good. The measured electron temperature profile is broader with a faster current ramp-up (Fig. 7, top panel). The higher temperature in the outer part of the plasma column increases the delay of the inward diffusion of plasma current leading to the formation of a broader current density profile during the current ramp up (Fig. 7, middle panel) and slower reduction of the $q_0$ (Fig. 7, bottom panel) in #72464. The ohmic heating profile is more off-axis in this case which contributes to the broadening of the $T_e$ profiles. Alternatively, the ohmic current diffuses inward faster in the cooler outer half of the plasma column in the discharge with slow current ramp-up producing a faster reduction of $q_0$ (Fig. 7, bottom) and triggering the sawtooth oscillations earlier. Indeed, the soft X-ray emission indicates that the first sawtooth crash occurs at 5.55 s in #72465, while there are no sawtooth oscillations during the current ramp-up phase in #72464. Thus, the non-linear coupling between the electron temperature and current, via the temperature dependent current conductivity and current dependent ohmic heating, can explain a slower reduction of the $q_0$ at faster current ramp-up (this coupling is even more complicated when the thermal electron diffusivity $\chi_e$ depends on the $q$-profile).

The electron density scan at fixed current ramp rate has been performed by varying the deuterium gas puff. The density effect on the internal inductance $l_i$ estimated with EFIT has been discussed in Ref. [3] where the achievement of similar $l_i$ in discharges with different plasma density has been explained by the simultaneous reduction of the electron temperature and $Z_{eff}$ with density leading to the unchanged current conductivity. The current diffusion simulations performed here confirm the interpretation given in Ref. [3]. Indeed, the simulated $q$-profiles are similar in three

discharges performed at different density and same current ramp rate (#72467, 72504 and 72723) where both $T_e$ and $Z_{eff}$ reduce with density (table 1). The first two discharges in table 1 (#72460 and 72464) illustrate a different situation where the electron temperature reduces with density, while $Z_{eff}$ slightly increases. The TRANSP simulations performed with a flat $Z_{eff}$ profile indeed show that the $q_0$ reduces slightly faster in discharge with higher density.

The auxiliary heating delays the reduction of $q_0$ in the analysed discharges which is confirmed also by a later appearance of sawtooth oscillations. The first sawtooth crash occurs at 7.46 s in the discharge with central ICRF heating (#72507) while the reference OH discharge (#72467) and the discharge with an off-axis heating (#72505) display the small-amplitude frequent sawtooth oscillations much earlier. The simulations of the current diffusion in #72507 show that both the higher electron temperature and lower core impurity concentration (an off-axis $Z_{eff}$ profile has been used) contribute to the delay of current penetration maintaining the $q_0$ above 0.7 till the time of the first sawtooth crash. Interestingly, a relatively long phase with a slightly reversed $q$-profile (till 6 s) has been obtained in simulations of this discharge (Fig. 8). During this phase the initially broad region of negative shear shrinks and the minimum safety factor reduces as current diffuses inward leading to the monotonic $q$-profile after 6 s (Fig. 8). The existence of the reversed $q$-profile in #72507 is justified also by Alfven cascades [21] which have been clearly observed in this discharge till 6 s. In the discharge with the off-axis ICRF heating a monotonic $q$-profile has been obtained during the whole current ramp up phase and the Alfven cascades were not observed. The initially reversed $q$-profile evolves rapidly to the monotonic shape also in the analysed OH discharges (before 2.7 – 2.9 s with $dI_{pl}/dt$ = 0.36 MA/s and even earlier in other discharges). Thus, in the analysed database the central ICRF heating

even at a relatively low power (3 MW) provides a unique opportunity to maintain the reversed $q$-profile for up to 70% of the duration of the current ramp up phase.

It should be mentioned also that the off-axis shape of $Z_{eff}$ used for the ICRF heated discharges does not help to maintain a higher $q_0$ for a longer time in the OH discharges. The electron temperature is lower in ohmic discharges, the inward current diffusion is faster and the current density profile is closer to the stationary than in the ICRF heated discharges. In this case a centrally peaked $Z_{eff}$ profile leading to a broader current density profile makes the $q_0$ evolution more consistent with the observed first sawtooth crash, while the off-axis $Z_{eff}$ profile leads to a very rapid $q_0$ reduction.

The NBI heated discharges have longer sawtooth free current ramp up phase than the OH discharges due to a higher electron temperature. The fraction of the beam driven current estimated with the NUBEAM module [22] in TRANSP is not significant at low NBI power (#72516) reducing from 8 - 9% at the beginning, to 6 - 7% at the end of the current ramp. At high NBI power (#72512) the beam driven current reaches 23 - 25% at the beginning of the current ramp up, and reduces to 15% by the end of the ramp up phase. The bootstrap current estimated with NCLASS varies from 4 - 5% at low ICRF and NBI power up to 12% obtained with the steep temperature profiles at high NBI power. The flux consumption reduces during the current ramp up phase by 25% - 46% when the neutral beam injection with powers in the range 4 - 9.8 MW are applied.

## V. Validation of transport models

The validation of the transport models in the self-consistent simulations of the plasma equilibrium, electron temperature and current density evolution has been performed with the ASTRA code. The current diffusion has been simulated using the NCLASS module for the neoclassical current conductivity and bootstrap current. The electron and impurity density and toroidal rotation velocity (when available) have been prescribed. The ion temperature has been simulated in the NBI heated discharges only where it can be compared with measurements and the model for the thermal ion diffusivity can be properly validated. The prescribed ion temperature constrained by the data consistency analysis has been used for other discharges. The heating sources (NBI and ICRF) have been taken from the interpretative TRANSP simulations while the OH heating power has been simulated with ASTRA. The Bohm-gyroBohm [11], GLF23 [14] and Coppi-Tang [9] models for thermal diffusivity have been tested. The predictive accuracy of transport models have been estimated for the time interval [$t_1$, $t_N$] in the time dependent simulations by using the following expressions:

$$rms = \left[ \frac{1}{N \cdot M} \sum_{t_n = t_1}^{t_N} \sum_{x_m = 0}^{x_m = 0.7} \frac{\left\{ T_{\exp}\left(t_n, \rho_m\right) - T_{sim}\left(t_n, \rho_m\right) \right\}^2}{T_{\exp}\left(t_n, \rho_m\right)^2} \right]^{1/2}$$

$$offset = \frac{1}{N \cdot M} \sum_{t_n = t_1}^{t_N} \sum_{x_m = 0}^{x_m = 0.7} \frac{T_{\exp}\left(t_n, \rho_m\right) - T_{sim}\left(t_n, \rho_m\right)}{T_{\exp}\left(t_n, \rho_m\right)}$$

Here $t_N$ is the end of the ramp up phase, $T_{exp}$ and $T_{sim}$ stand for the experimental and simulated electron and ion temperatures respectively, $N = (t_N - t_1)/\Delta t_{output}$ is the number of the time slices, $\Delta t_{output} = 0.1$ s is the output time interval, $M$ is the number of radial points in the interval $0 \le \rho_m \le 0.7$. The choice of the simulation start time $t_1$ and boundary temperature is discussed below.

### *a) ohmic plasmas*

The OH discharges have been simulated starting from 2 - 2.2 s, till the end of the current ramp up. The simulations have been performed with the Bohm-gyroBohm and Coppi-Tang models since these models do not depend on the ion temperature, that is not measured in ohmic plasmas. The electron temperature and current density evolution has been simulated under various assumptions for $T_i$, $Z_{eff}$ and radiative power profile $P_{rad}$.

The choice of the radial simulation region for the thermal energy equation is a sensitive point of the modelling, due to a poor edge data quality after the breakdown. The Thomson scattering measurements of electron density are not available for the periphery plasma region during the first few seconds of the current ramp up phase where the outmost data point of the Thomson scattering measurements is located around $\rho$ = 0.8 – 0.85. The uncertainty in the plasma density outside this radius strongly affects the modelling results with the Bohm-gyroBohm transport coefficients depending on the electron density gradient via the $\nabla p_e$ term (here $p_e$ is thermal electron pressure). For example, when the outmost measured value of the density is extrapolated over the region $\rho$ = 0.85 – 1 (i.e., the density profile is flat near the edge) the electron temperature outside $\rho$ = 0.85 is strongly over-predicted in simulations with the Bohm-gyroBohm model. The discrepancy between the measured and simulated temperature reduces when a density at the plasma periphery, linearly decaying towards the edge, is used. By contrast, the Coppi-Tang transport coefficients, which are generally strongly increasing towards the edge due to the inverse density dependence and geometrical factor, are less sensitive to the density extrapolation and provide a better agreement with the measured $T_e$ outside $\rho$ = 0.85 in

simulations performed for the whole plasma region. Keeping in mind a strong effect of the uncertainty in edge density profile on the modelling results obtained with the Bohm-gyroBohm model, the validation of this model has been performed for the plasma region $\rho$ = 0 - 0.85, i.e. the temperature measured at $\rho$ = 0.85 is used as a boundary temperature. In case of the Coppi-Tang model, the thermal diffusivity slightly inside $\rho$ = 0.85 is not always consistent with the computed diffusivity leading to a hollow $T_e$ profile near the boundary due to large edge transport. Trying to avoid this inconsistency and illustrate the best capability of the Coppi-Tang model this model has been tested for the whole plasma region taking the boundary condition at $\rho$ = 1.

The results of the validation of the Bohm-gyroBohm model for the OH discharges are summarised in table 3. The sensitivity of the predictive accuracy to various assumptions on the non-measured quantities has been investigated in these simulations. The first column of table 3 shows the modelling results obtained with the prescribed ion temperature matching the measured neutron yield, peaked $Z_{eff}$ profile providing the $q_0$ evolution consistent with the time of the first sawtooth crash and flat radiative power profile consistent with the total measured radiative power. The flat $P_{rad}$ profile has been replaced with a peaked profile in the simulations shown in the second column. This time-evolving profile has been calculated in ASTRA using the atomic data of Ref. [23] and constraining the total radiative power by its measured value. The predicted on-axis $P_{rad}$ profiles have a nearly parabolic shape with a half-width of (0.3-0.5)$\rho$. The third column of table 3 shows the results obtained with a flat $Z_{eff}$ profile which causes a too rapid reduction of $q_0$ in the current diffusion simulations. In all simulations the sawtooth mixing of current density has been taken into account preventing the reduction of the central $q$ below 0.8. The predictive

accuracy of the transport models is shown in table 3 separately for the sawtooth-free time interval and for the whole current ramp up phase for discharges with the sawtooth crashes.

The modelling shows that the Bohm-gyroBohm thermal diffusivity under-predicts the thermal electron transport, under various assumptions for the non-measured data, with the *rms* deviation between the measured and simulated temperature reaching 46% in some cases (table 3 and Fig. 9, dashed curves). The variation of the radiative power profile (the total radiative power in these discharges is 5-12% of the OH power) or $Z_{eff}$ profile does not change the results significantly. Since the predictive accuracy of the Bohm-gyroBohm model for OH discharges appears to be unsatisfactory, an attempt to re-normalise this model has been made. The Bohm-like (dominant) term in this model has been multiplied by a constant in time coefficient $C_{e,BgB}$ and this coefficient has been adjusted to obtain a better match of measured temperature in the simulations with peaked $Z_{eff}$ and flat $P_{rad}$ (first column in table 3). The best agreement with the measured electron temperature characterised by the *rms* deviation varying within 11.4% for the OH discharges considered has been found in simulations with $C_{e,BgB}$ = 3.3 (table 3, fourth column and Fig. 9, solid curves). No particular correlation of the modelling accuracy with the plasma density and current ramp rate has been found with the re-normalised Bohm-gyroBohm model although a weak correlation with the current ramp rate showing a better prediction in discharges with faster current ramp up can be seen in simulations with peaked radiative power (second and third columns in table 3).

The electron temperature profiles measured with the Thomson scattering diagnostics are generally broader than the ECE temperature profiles. In some cases the electron temperature predicted with the original Bohm-gyroBohm model matches

the Thomson scattering data better than the re-normalised model (Fig. 9 top). However, for the majority of discharges the measured profiles are better predicted with the re-normalised Bohm-gyroBohm model (Fig. 9, bottom panel shows such an example).

The results shown in table 3 have been obtained using the $T_i/T_e$ ratio matching the measured neutron yield in simulations with peaked $Z_{eff}$ profile. This ratio is equal to one for all analysed discharges except the low density discharge 72460 where it reduces down to 0.67. To check the sensitivity of the $T_e$ prediction in #72460 to ion temperature the modelling with the re-normalised Bohm-gyroBohm model has been performed assuming $T_i/T_e$ = 1 and using the peaked $Z_{eff}$ and flat radiative power profile. The obtained results (*rms* = 8.9%, *offset* = 6.8%) show that the *rms* deviation and offset are weakly sensitive to the $T_i/T_e$ ratio, which may be explained by a relatively small contribution of the electron-ion collisional energy exchange to the energy balance.

The same assumptions on the input data have been used for the validation of the Coppi-Tang model. Larger disagreement between the simulations with this model and measurements due to the strongly overestimated temperature has been obtained as compared to the original Bohm-gyroBohm model (table 4). The predicted electron temperature is sensitive to the radiative power profile - the *rms* deviation reduces by nearly 20% when the flat profile of the radiative power was replaced with a peaked profile (table 4, second column). The change of $Z_{eff}$ profile from flat to peaked weakly affected the predictive accuracy. Figure 10 illustrates the typical discrepancy between the simulated and measured electron temperature. The thermal electron diffusivity computed with the Coppi-Tang model is large near the edge providing a good agreement with a measured temperature at the plasma periphery, but it strongly

reduces inward (for example, $\chi_e$ = 0.1 - 0.16 $m^2$/s at mid-radius in simulations shown by the dashed curves in Fig. 10 as compared to 2.7 – 4 $m^2$/s obtained with the re-normalised Bohm-gyroBohm model reasonably predicting the measured temperature). With such small values of thermal diffusivity an off-axis peaked temperature profile forms due to the initially off-axis OH heating profile and this peaked off-axis $T_e$ profile is maintained for a long time. Similar to the Bohm-gyroBohm model the Coppi-Tang model has been re-normalised by multiplying it by a constant coefficient $C_{e,CT}$ and this coefficient has been adjusted to minimise the discrepancy with the measured temperature in the OH discharges. It was found that an increase of the Coppi-Tang thermal electron diffusivity by factor 8 is needed for a more accurate prediction of electron temperature in the analysed OH pulses (table 4, third column and Fig. 10, solid curves). The *rms* deviation between the simulated and measured temperature obtained with $C_{e,CT}$ = 8 is still larger than the *rms* deviation obtained with the re-normalised Bohm-gyroBohm model.

The electron temperature predicted with two empirical models is strongly sensitive to $Z_{eff}$. By artificially reducing $Z_{eff}$ by 40% and re-adjusting $Z_{eff}$ profile to maintain the $q_0$ above one till the time of the first sawtooth crash, a much more accurate temperature prediction has been obtained with the original Bohm-gyroBohm model for the OH pulses (*rms* = 4.6 – 14.5% with $C_{e,BgB}$ = 1 in this case). The inward current diffusion slows down with reduced $Z_{eff}$ leading to a larger safety factor in the core region and increasing the $q^2$-dependent Bohm-gyroBohm thermal diffusivity. The *rms* deviation obtained with the original Coppi-Tang model also reduces at lower $Z_{eff}$ (*rms* ≤ 75.6%), but it is still much larger than the *rms* deviation obtained with the Bohm-gyroBohm model.

### *b) ICRF heated plasmas*

In these discharges the ICRF power exceeds the OH power by an order of magnitude. The ICRF power deposition has been simulated with the TORIC code [24] in TRANSP assuming 63 poloidal and one toroidal harmonic. The typical electron and ion heating profiles obtained with the off-axis $Z_{eff}$ profile and $T_i/T_e$ ratio, matching the measured neutron yield, are shown on Fig. 11. In two analysed ICRF heated discharges the ion cyclotron waves produce mainly electron heating (78 - 80% of the ICRF power is absorbed on electrons). The collisional slowing down of the hydrogen minority on electrons is the dominant heating mechanism. The direct electron heating (Landau damping) is small in the discharge with the on-axis resonance position (less than 7% of the total ICRF power) where about 90% of the ICRF power is absorbed by the hydrogen minority. With the off-axis resonance position 77% of injected power is absorbed by hydrogen minority. The remaining power is damped on electrons inside the mid-radius (Fig. 11, red solid curve). The thermal ions are heated by collisions with hydrogen minority ions; the direct ($2^{nd}$ harmonics) ion heating is negligible in these discharges.

The sensitivity of the electron and ion ICRF heating profiles to $Z_{eff}$ and ion temperature has been examined by varying the $Z_{eff}$ profile from the off-axis to flat and by increasing the $T_i/T_e$ ratio from 0.6 to 1. The total electron and ion power weakly varies in these simulations (within 1-1.5%). The biggest local change of the heating with the variation of $Z_{eff}$ has been obtained in the core for #72507 (the electron heating increases nearly by 15% and the ion heating reduces by about 30% with an increase of the core $Z_{eff}$ from 1 to 2.5). The sensitivity of the heating profiles to the variation of ion temperature is much weaker than to the $Z_{eff}$ variation.

The transport simulations have been performed using the ICRF heating profiles computed by TORIC, Abel inverted radiative power profiles, available for the ICRF heated discharges, off-axis $Z_{eff}$ profile and $T_i/T_e$ ratio matching the measured neutron yield. Similar to the OH plasmas, the original Bohm-gyroBohm model strongly underestimates the thermal electron transport in the discharge with the off-axis heating while the re-normalised Bohm-gyroBohm model with the same coefficient as for the OH plasmas ($C_{e,BgB}$ = 3.3) satisfactory predicts the electron temperature profile in this discharge (Fig. 12 top and table 5). In discharge with the central heating the electron temperature is predicted relatively accurately with the original Bohm-gyroBohm model outside $\rho$ = 0.2, but the core temperature is under-predicted (Fig. 12, bottom panel). The re-normalised Bohm-gyroBohm model ($C_{e,BgB}$ = 3.3) under-predicts the core temperature in a broader region (Fig. 12, bottom panel).

The original Coppi-Tang model strongly underestimates the thermal electron transport in the considered ICRF heated plasmas with the *rms* deviation exceeding 100%. The *rms* deviation has been reduced to 26.6% for #72505 and to 41% for #72507 and the electron temperature was under-predicted when the same multiplier as for the OH plasmas ($C_{e,CT}$ = 8) has been used. A much better agreement with the measured electron temperature in #72505 has been obtained by using $C_{e,CT}$ = 4.9 (Fig. 12, top panel and table 5), but the strong central temperature peaking in #72507 was not predicted accurately with this coefficient (Fig. 12, bottom panel) increasing the *rms* deviation. The predictive accuracy of this model for the discharge with central heating can be improved by reducing the calibration coefficient to $C_{e,CT}$ = 3.5. The *rms* deviation and offset obtained with this calibration coefficient (12.12% and 0.34% correspondingly) are similar to the *rms* deviation and offset obtained with the Bohm-gyroBohm model for this discharge.

### *c) NBI assisted current ramp up*

In the ICRF heated discharges the electron heating was dominant while in the NBI heated discharges it is nearly equal (#72516) or smaller (#72511 and 72512) than the ion heating during the NBI flat-top. Since the NBI heated discharges are performed at low density the NBI power is deposited mainly in the core region (Fig. 13), but the electron heating profile is broader than the profile obtained with the central ICRF heating (45 - 50% of the total auxiliary electron heating power is absorbed within $\rho = 0.4$ with NBI heating while this fraction increases to 85 - 95% in the discharge with the on-axis ICRF heating).

The results of the validation of the original Bohm-gyroBohm and GLF23 model are presented in table 6 and illustrated in Fig. 14. The electron and ion temperature are predicted within 10% of the *rms* deviation from the measured profiles with both models in the low power discharge 72516. The ion temperature is predicted slightly more accurately with the GLF23 model while the electron temperature is better predicted with the Bohm-gyroBohm model in this discharge. The discrepancy between the GLF23 model prediction and measurements increases in discharges with higher power (table 6). The simulated electron temperature profiles are typically slightly more peaked than the measured profiles (Fig. 14, bottom left panel) while the ion temperature is sometimes strongly overestimated (Fig. 14, bottom right panel). It should be mentioned that the *ExB* shear has been computed in the GLF23 model using the toroidal, diamagnetic and neoclassical poloidal rotation since the measurements of the poloidal rotation are not available for analysed discharges. The degradation of the predictive accuracy of the Bohm-gyroBohm model with heating power is less pronounced although the *rms* deviation is larger for #72512 than for other discharges.

The overall agreement with measurements for the selected group of the NBI heated discharges is satisfactory for this model (*rms* is within 15%).

Figure 14 includes also the results obtained with the re-normalised Coppi-Tang model. As for the other analysed discharges the original Coppi-Tang model strongly overestimates both electron and ion temperature in these NBI heated pulses. Following the same approach as for other discharges this model has been re-normalised and the constant coefficient minimising the *rms* deviation over the group of the NBI heated discharges has been determined. The most accurate $T_e$ and $T_i$ prediction has been obtained by using $C_{e,CT} = 4.7$ (which is close to the normalisation coefficient obtained for the off-axis ICRF heated discharge) and $C_{i,CT} = 8$ (table 6). The *rms* deviation obtained with the re-normalised Coppi – Tang model does not exceed 12.6% for discharges considered that is comparable with the Bohm-gyroBohm predictive accuracy.

Summarising the results of this section, the original Bohm-gyroBohm model predicts relatively accurately the thermal transport in the discharges with central heating. The thermal electron transport in the OH plasmas is underestimated with this model by a factor of 3.3, but this factor is highly sensitive to the effective charge of plasma in the self-consistent simulations of temperature and current density evolution. Taking into account this factor in the modelling of the OH and off-axis ICRF heated plasmas, the Bohm-gyroBohm model predicts electron and ion (for the NBI heated plasmas) temperature with *rms* < 15%. The predictive accuracy of the GLF23 model for the NBI heated discharges is within 28.17% of the *rms* deviation from the measurements being rather accurate for the low power discharges and increasing with power. The Coppi-Tang model strongly overestimates the temperature in the considered discharges, but its predictive accuracy can be significantly improved by

multiplying the computed thermal electron diffusivity by factor 8, 4.7 and 4.9 for the OH, off-axis ICRH and NBI heated plasmas correspondingly (the *rms* deviation is within 31.2%, 7% and 9% respectively in these cases). The strongly peaked core electron temperature is under-estimated with the re-normalised Coppi-Tang model when the normalisation coefficient determined for the other auxiliary heated discharges ($C_{e,CT}$ = 4.7 – 4.9) is applied. The ion temperature in the NBI heated discharges is predicted accurately with the Coppi-Tang model when the re-normalisation coefficient $C_{i,CT}$ = 8 is used (the *rms* deviation is less than 12.6%).

## VI. Modelling of the current ramp up in ITER

The simulations of the current ramp up in ITER are performed here in order to estimate the duration of the sawtooth-free current ramp up phase and a target $q$-profile formed at the end of the current ramp up in the baseline H-mode scenario with $q_{95}$ = 3 under different assumptions for thermal transport. As an example the auxiliary heated current ramp up with central electron heating (e.g. electron cyclotron heating (ECRH)) is considered. The GLF23 and original Bohm-gyroBohm model which provide an accurate temperature prediction in the JET discharges with central heating and do not require a re-normalisation are selected for this study. Since these two models predict different peaking of electron temperature it is interesting to investigate the effect of this difference on the scenario evolution.

Similar to the simulations of the JET discharges the plasma model used for ITER includes the equation for electron and ion temperature solved in the limited plasma region $\rho \leq 0.85$ and current diffusion equation solved in the region $\rho \leq 1$. A low temperature at the simulation boundary (with $T_i = T_e$ at $\rho \geq 0.85$), rising linearly

with plasma current from 100 eV to 550 eV during the current ramp up, and a linear temperature profile outside $\rho$ = 0.85, decreasing towards the edge, have been assumed. The simulations have been performed with a prescribed Greenwald fraction of electron density taking for example $n_e/n_{Gr}$ = 0.5 (i.e. electron density increases with plasma current) and a parabolic density profile. Deuterium plasmas with 2% of Be and 0.12% of Ar impurity have been considered and the radiative losses caused by these impurities have been included in the electron energy equation. Current diffusion has been simulated using NCLASS [18] for the bootstrap current and current conductivity. The ECRH heating profile has been mimicked by imposing a central Gaussian with the width $\Delta\rho$ = 0.2.

The simulations of the current ramp up are started in a small circular OH plasma ($a$ = 1.6 m) at magnetic field $B_t$ = 5.3 T and plasma current $I_{pl}$ = 0.5 MA. The plasma expands to the full volume ($a$ = 2 m, $\kappa$ = 1.8 and $\delta$ = 0.39) at 16 s when $I_{pl}$ = 4.64 MA and the plasma current reaches its nominal value 15 MA at 80 s (Fig. 15). The electron heating power $P_e$ has been applied at 3 s and raised linearly in time till 7 s to its stationary value, which is varied from 2 to 20 MW in different simulations. The initial OH phase has been simulated with the Bohm-gyroBohm thermal electron and ion diffusivity in order to provide similar target plasmas at the beginning of the auxiliary heating.

The effect of the electron heating and the sensitivity of the plasma evolution to the transport model are summarised in Fig. 16, showing the time when $q_0$ = 1 is achieved ($t_{q0=1}$), and the central electron and ion temperature at the end of the current ramp-up obtained in simulations with different heating powers and transport models. The bottom panel of Fig. 16 presents an example of the electron temperature profiles obtained at 7 s (start of the auxiliary power flat-top) and 80 s (end of the current

ramp-up) with 4 MW of applied power using different transport models. A clear difference in $t_{q0=1}$ has been obtained in simulations with different transport models at all applied powers (typically 14 – 19 s, Fig. 16, top) with a longer sawtooth-free period obtained with the GLF23 model. A similar central temperature at the end of the current ramp-up (but different $T_e$ peaking) has been obtained with two models at low power while the difference in predicted temperatures increases with power.

The difference in the temperature and current density evolution obtained with different transport models can be understood taking into account the parametric dependencies included in these models. When the auxiliary heating is applied both the Bohm-gyroBohm and GLF23 computed thermal diffusivities increases. This increase is caused by the rising electron pressure in the Bohm-gyroBohm model [11] and by the rising ion temperature gradient in the GLF23 model (where the ITG instability was dominant at the beginning of electron heating) caused by the electron-ion energy exchange. During the rise of heating power (3 – 7 s) the GLF23 model predicts lower diffusivities than the Bohm-gyroBohm model, particularly near the plasma periphery (the GLF23 transport coefficients reduces towards the edge while the Bohm-gyroBohm transport increases). The electron temperature predicted with the GLF23 model is higher (Fig. 16 bottom panel, solid curves) and the inward diffusion of the ohmic current is slower than in simulations with the Bohm-gyroBohm model. Starting from the power flat-top (7 s) until the end of the current ramp-up the Bohm-gyroBohm transport coefficients reduce slowly due to the relaxing $q$-profile ($\chi_{BgB} \sim q^2$). The evolution of the GLF23 transport coefficients depends on the applied power. At low power ($P_e$ < 8MW) the ITG instability remains a dominant drive of the anomalous transport till the end of the current ramp up. When the applied power exceeds 8 MW the rapidly rising electron temperature triggers the transition from the

ITG to the TEM-driven anomalous transport during the power ramp up. The phase with the dominant TEM transport is transient and relatively short (4 - 10 s depending on the heating power applied). It is terminated with increased density, which enhances the electron-ion energy exchange and increases the ion temperature. Then, the ITG mode becomes the dominant instability till the end of the current ramp-up. The reducing Bohm-gyroBohm thermal diffusivities become comparable with the GLF23 diffusivities around 9 – 11 s. The higher electron temperature obtained with the GLF23 model before this time produces an important delay in the $q_0$ reduction leading to a large $t_{q0=1}$ (Fig. 16, top panel). The $q$-profile has a monotonic shape during the current ramp-up in all simulations except the 20 MW heating case simulated with the GLF23 model where the $q$-profile in the outer part of plasma was transiently reversed. The current density profiles obtained with the Bohm-gyroBohm and the GLF23 model at the end of the current ramp-up are different. The current mixing radius estimated with the Kadomtsev reconnection model is larger by up to 14 cm (the largest difference is obtained at 20 MW) in simulations with the Bohm-gyroBohm model.

An interesting peculiarity of the results obtained with the Bohm-gyroBohm model is a non-monotonic dependence of the $t_{q0=1}$ on the heating power (Fig. 16, top panel, black symbols). The time evolving $q_0$ and the current density profiles in the OH and auxiliary heated plasmas obtained with 4 and 16 MW of applied power are compared in Fig. 17. Generally, the auxiliary electron heating is supposed to delay the inward current diffusion and to increase the duration of the phase with $q_0 > 1$. This effect is clearly seen in simulations with the GLF23 and Bohm-gyroBohm model at $P_e > 5$ MW (Fig. 16, top panel). A more detailed comparison of the $q_0$ evolution in OH and auxiliary heated plasmas with $P_e$ =16 MW is given in Fig. 17 (top panel). To

understand the reasons for the opposite heating effect obtained at a low power one should take into account the influence of the temperature peaking on the final stationary magnetic equilibrium. Since the stationary electron temperature profile obtained with the central heating would be more peaked in the absence of the sawtooth oscillations than the OH temperature profile, the stationary $q$-profile would be also more peaked in this case. With 4 MW of heating power, which does not produce a sufficient delay of the current diffusion, but forms a peaked temperature and current density profile very rapidly (Fig. 17, bottom left panel) the $q_0$ reduction occurs even faster than in the otherwise similar OH plasma (Fig. 17, top panel, dotted-dashed and solid curves). The current density profile obtained at the end of the current ramp up would be even more peaked with 16 MW of applied power if this peaking would not be prevented by the sawtooth mixing which produces a larger mixing radius in this case than in OH and low power heated plasmas (Fig. 17, bottom right panel).

## VII. Summary and discussion

A data consistency analysis, and the transport and current diffusion modelling of the current ramp-up in an ITER demonstration discharges performed at JET have been carried out, in order to estimate the predictive accuracy of different models for thermal transport. The selected database includes OH plasmas with a range of electron density and current ramp rate as well as auxiliary heated discharges with various heating profiles (on-axis and off-axis ICRF heating) and powers (NBI heating). The collected experimental database is of interest for the modelling since it allows one to test the models under different conditions, to clarify the effects produced by a

variation of a single parameter on the scenario evolution and to check the correlation of the predictive accuracy of transport models with various parameters. Such a correlation (if it is found) would help to improve the transport models.

The particular emphasis of this study is on data consistency. Taking the relatively poorly diagnosed OH and ICRF heated plasmas (no measured $T_i$ or $Z_{eff}$ profiles) as an example, the complexity of the data consistency analysis is described to show the uncertainties in the data that are important for the transport model validation, and the ways to constraint these uncertainties. For the JET discharges considered, the non-measured quantities include the profile of the effective charge of plasma, ion temperature and toroidal rotation. The ion temperature and effective charge have been adjusted here to match the measured neutron yield and the time of the first sawtooth crash determined from the soft X-ray emission measurements. The estimated range for the non-measured quantities has been taken into account in the estimation of the predictive accuracy of the transport models by performing a sensitivity study.

Taking into account the data consistency constraints the effects of the current ramp rate, plasma density and auxiliary heating on the current diffusion have been investigated. The beneficial effect of the faster current ramp up on the duration of the sawtooth-free phase in OH discharges has been observed experimentally and reproduced in the simulations of the current diffusion performed with measured electron temperature. The broader $T_e$ profiles and slower $q_0$ reduction in discharges with a faster current ramp up (#72460 and 72464) can be partly explained by a strong coupling between the plasma current, electron temperature and ohmic heating, when a faster current and OH power rise at the plasma periphery increase the electron temperature locally, which in its turn further delays the inward current diffusion

maintaining the off-axis heating and current profile for a longer time. This coupling can be further enforced by a $q$-dependent thermal electron diffusivity. No density effect on the current diffusion has been found in the discharges, for a current ramp rate of 0.28 MA/s. As explained in Ref. 3 the reduction of $Z_{eff}$ with density compensates the reduction of the current conductivity caused by a lower temperature in high density plasmas, leading to similar current density profiles and internal inductance in discharges with different plasma density. The auxiliary central heating (ICRF and NBI) efficiently delays the reduction of the $q_0$ in the analysed discharges. With 3MW of central ICRF heating the reversed $q$-profile has been maintained till 6 s and the sawtooth-free phase was much longer in this pulse than in the reference OH discharge. In other analysed discharges the initially reversed $q$-profile evolves rapidly to be monotonic (before 3 s). Thus, the central ICRF heating even at a relatively low power is an efficient tool for maintaining the reversed $q$-profile for up to 70% of the duration of the current ramp up phase. The NBI heating also delays the current diffusion producing a sawtooth-free current ramp-up, but a higher NBI power is needed in this case ($P_{NBI} \geq 7$ MW in corresponding discharges).

Three transport models for thermal diffusivity - the empirical Bohm-gyroBohm [11] and Coppi-Tang [9] model, and the theory-based GLF23 model [14] - have been tested for selected discharges. The results of the validation of these models can be summarised as follows:

- The Bohm-gyroBohm model predicts accurately the temperature evolution in the $L$-mode plasmas with central heating (on-axis ICRF and NBI heating) with the *rms* deviation less than 15%. The electron temperature in the OH and off-axis ICRF heated discharges is over-predicted with this model (*rms* = 17 – 46% for different discharges);

- the GLF23 model tested for the NBI heated discharges, with available $T_i$ measurements, predicts accurately the temperature evolution in the low power NBI heated discharge (*rms* ≤ 10%) while its predictive accuracy reduces with heating power (*rms* error increases up to 28.2% at 9.8 MW). It is worth mentioning that the $E \times B$ shear in the GLF23 model has been estimated with the neoclassical poloidal rotation since the measurements of the poloidal rotation are not available for analysed discharges;

- the Coppi-Tang model strongly overestimates the temperature in all discharges considered;

- a possibility to improve the predictive accuracy of the empirical models by multiplying them by a constant coefficient (the Bohm-like term has been multiplied in case of the Bohm-gyroBohm model) minimising the *rms* deviation within each group of discharges with the same heating method has been tested. It has been found that

(a) a fixed multiplier in the Bohm-gyroBohm model ($C_{e,BgB} = 3.3$) reduces the *rms* deviation to 5 – 11.4% both in OH and off-axis ICRF heated discharges;

(b) the optimised re-normalisation coefficient in the Coppi-Tang model in OH plasmas is $C_{e,CT} = 8$, but the overall prediction accuracy obtained with this coefficient is lower (*rms* ≤ 31.2%) than with the re-normalised Bohm-gyroBohm model indicating that a more complicated parametric dependence is needed for the Coppi-Tang model;

(c) in the auxiliary heated discharges the re-normalisation coefficient in the Coppi-Tang thermal electron diffusivity should be reduced to 4.7 – 4.9. An accurate temperature prediction has been obtained with this re-

normalisation (*rms* ≤ 9%) in all auxiliary heated discharges except the discharge with the on-axis ICRF heating where the steep core temperature profile was not predicted;

(d) the thermal ion diffusivity in the Coppi-Tang model should be reduced by a factor 8 ($C_{i,CT}$ = 8) in the NBI heated discharges (*rms* < 12.6% in this case).

Although the discrepancy between the predicted and measured temperature in the OH discharges is larger in the simulations with the Coppi-Tang model than with the Bohm-gyroBohm model, the advantage of the Coppi-Tang model is a low sensitivity to the boundary density which makes it applicable for the whole plasma region. The temperature simulated with the Bohm-gyroBohm and the GLF23 models is strongly sensitive to the boundary conditions and these models have not been tested outside $\rho$ = 0.85 where the data quality after the breakdown is poor.

The predictive accuracy for the OH and ICRF heated plasmas discussed above has been obtained under the "reference" assumptions of a shaped $Z_{eff}$ profile, providing the $q_0$ evolution consistent with the time of the first sawtooth crash, and ion temperature, matching the measured neutron yield. By performing the sensitivity study it was found that the electron temperature simulated with both empirical models is highly sensitive to $Z_{eff}$. When $Z_{eff}$ has been reduced by 40% a much more accurate prediction of the temperature evolution has been obtained with the original empirical models (*rms* ≤ 15% with the Bohm-gyroBohm model and *rms* = 34 - 75% with the Coppi-Tang model). The re-normalisation of the Bohm-gyroBohm model was not needed in this case. The variation of the $Z_{eff}$ and radiative power profile from peaked to flat has less effect on the modelling results obtained with the Bohm-gyroBohm model (the variation of *rms* is within 5%). The original Coppi-Tang model is sensitive

to the variation of radiative power profile with the *rms* deviation reducing by up to 20% with a peaked $P_{rad}$.

Based on the transport model validation performed for the JET discharges the modelling of the current ramp-up for ITER has been carried out with a particular emphasis on the sensitivity of the plasma evolution during the current ramp-up to the transport model. The GLF23 and original Bohm-gyroBohm model have been used in these simulations. Similar to the JET discharges the current ramp-up in a large plasma volume, with $q_{95} = 3$ achieved at the current flat top (i.e. baseline H-mode scenario), has been considered and the scan in the electron heating power varying within the range 2 - 20 MW has been performed.

At low electron heating power ($P_e < 8$ MW) similar central temperatures have been obtained with the two selected transport models at the end of current ramp-up, with a slightly broader $T_e$ profile obtained with the Bohm-gyroBohm model. This is equivalent to the temperature prediction obtained with these two models for the JET discharge with low NBI heating power. It should be mentioned that the other predictive simulations comparing the Bohm-gyroBohm model with the Multi-Mode-95 transport model, which is based on the similar drift mode physics as the GLF23 model, show that the modelling results match experimental data about equally well for the L-mode DIII-D and TFTR discharges [25] and H-mode JET and DIII-D discharges [26]. The heating power scan performed here for the ITER current ramp-up phase shows that a clear difference in the temperature predicted with two transport models appears at high heating power - the Bohm-gyroBohm model gives a higher prediction for the central electron temperature than the GLF23 model.

The GLF23 and Bohm-gyroBohm models predict different transient temperature evolution with a higher $T_e$ obtained with the GLF23 model after the start

of auxiliary heating. This difference in the transient behaviour makes a strong impact on the $q$-profile evolution extending the phase with $q_0 > 1$ up to 19 s in simulations with the GLF23 model. Assuming the Kadomtsev reconnection model for the sawtooth crashes a broader current mixing region has been obtained with the Bohm-gyroBohm model (by 14 cm at $P_e$ = 20 MW). Finally a clear non-monotonic dependence of the duration of the phase with $q_0 > 1$ has been found in simulations with the Bohm-gyroBohm model, which is different with the GLF23 simulations and can be indirectly used for the distinguishing between these two models in future experiments.

Summarising the ITER modelling results, the duration of the current ramp-up phase has been increased from 17 – 31 s to 34 – 50.5 s (the uncertainty in these estimations depends on the transport model applied) by increasing the central electron heating from 2 to 20 MW. A further increase of this phase could be achieved by accessing the broader H-mode like temperature profiles, as done in JET experiments, or by applying the lower hybrid current drive during the current ramp up [27].

## Acknowledgements

Drs. C. Angioni, C. E. Kessel, A. R. Polevoi and T. C. Hender are warmly acknowledged for useful discussions and comments. This work was done under EFDA and partly funded by the United Kingdom Engineering and Physical Sciences Research Council under grant EP/G003955 and the European Communities under the contract of Association between EURATOM and CCFE. The views and opinions expressed herein do not necessarily reflect those of the European Commission

## References


1. G L Jackson, T A Casper, T C Luce *et al*, Nucl. Fusion **48** (2008) 125002

2. H Zohm, J Adamek, C Angioni *et al*, "Overview of ASDEX Upgrade results", 22nd IAEA 2008, Geneva, paper OV/2-3

3. A C C Sips, T A Casper, E J Doyle *et al* "Studies for the current rise phase in ITER Experiments and Modelling", 22nd IAEA 2008, Geneva, paper IT/2-2 and submitted to Nucl. Fusion

4. C E Kessel, D Campbell, Yu Gribov *et al*, "Development of ITER 15 MA ELMy H-mode Inductive Scenario", 22nd IAEA Conference, 2008, Geneva, paper IT/2-3

5. G M D Hogeweij, J Hobirk, F Imbeaux, *et al*, "Simulation of current ramp-up phase of ITER discharges", 34th EPS Conference on Plasma Phys., Warsaw, Poland, 2-6 July 2007

6. V Parail, P Belo, P Boerner *et al*, Nucl. Fusion, in press

7. Yu Gribov, D Humphreys, K Kajiwara *et al*, Nucl. Fusion **47** (2007) S385

8. E J Doyle, W A Houlberg, Y Kamada *et al*, Nucl. Fusion **47** (2007) S18

9. S C Jardin, M G Bell, N Pomphrey, Nuc. Fusion **33** (1993) 371

10. A Taroni, M Erba, E Springmann and F Tibone, Plasma Phys. Contr. Fusion **36** (1994) 1629

11. M Erba, T Aniel, V Basiuk *et al*, Nucl. Fusion **38** (1998) 1013

12. T J J Tala, V V Parail, A Becoulet et al, Plasma Phys. Contr. Fusion **44** (2002) 1181

13. R J Goldston, D C McCune, H H Towner, S L Davis, R J Hawryluk and G L Schmidt, J. Comp. Physics **43** (1981) 61

14. R E Waltz, G M Staebler, W Dorland, G W Hammett, M Kotschenreuther, and J A Konings, Phys. Plasmas **4** (1997) 2482

15. D P O'Brien, L L Lao, E R Solano *et al*, Nucl. Fusion **30** (1992) 1351

16. J Svensson, A Werner, "Large Scale Bayesian Data Analysis for Nuclear Fusion Experiments", Proceedings IEEE Workshop on Intelligent Signal Processing WISP 2007

17. J Svensson, A Werner, Plasma Phys. Control. Fusion **50** (2008)

18. W A Houlberg, K C Shaing, S P Hirshman, M C Zarnstorff, Phys. Plasmas **4** (1997) 3230

19. I Voitsekhovitch, B. Alper, M Brix *et al*, Nucl. Fusion **49** (2009) 055026

20. G V Pereverzev, P N Yushmanov, Report IPP 5/98, Max-Planck-Institute fur Plasmaphysik, 2002

21. S E Sharapov, B Alper, H L Berk *et al*, Phys. Plasmas **9** (2002) 2027

22. A Pankin, D McCune, R Andre *et al*, Comp. Phys. Comm. **159** (2004) 157

23. D E Post, R V Jensen, C B Tarter, W H Grasberger and W A Lokke, Atomic Data and Nuclear Data Tables, **20** (1977) 397-439

24. M Brambilla, Plasma Phys. Contr. Fusion **41** (1999) 1

25. T Onjun, G Bateman, A H Kritz, D Hannum, Phys. Plasmas **8** (2001) 975

26. D Hannum, G Bateman, J Kinsey *et al*, Phys. Plasmas **8** (2001) 964

27. I Voitsekhovitch, X Litaudon, D Moreau *et al*, Nucl. Fusion **37** (1997) 1715

Table 1. Parameters of the OH current ramp up discharges: current ramp rate, line averaged density, effective charge and electron temperature (ECE data) measured near the magnetic axis (3 m) at the end of the current ramp up.

| Shot | $dI_{pl}/dt$ MA/s | $n_l/10^{19}$ $m^{-3}$ | $Z_{eff}$ | $T_{e0}$ keV |
|---|---|---|---|---|
| 72460 | 0.36 | 1.0 | 2. | 2.5 |
| 72464 | 0.36 | 1.45 | 2.2 | 2.2 |
| 72465 | 0.19 | 1.42 | 2.2 | 2.1 |
| 72467 | 0.28 | 1.44 | 2.11 | 2.1 |
| 72504 | 0.28 | 2.0 | 2.06 | 1.8 |
| 72723 | 0.28 | 2.63 | 1.8 | 1.6 |

Table 2. Parameters of the NBI assisted current ramp up discharges: NBI power, line averaged density, effective charge and electron and ion temperature measured at 3 m at the end of the current ramp up.

| Shot # | $P_{NBI}$, MW | $n_l/10^{19}$ $m^{-3}$ | $Z_{eff}$ | $T_{ECE}/T_{CX}$ (keV) at 3m |
|---|---|---|---|---|
| 72516 | 4 | 1.76 | 2.4 | 4 / 4 |
| 72511 | 7 | 2.03 | 2.2 | 4.9 / 6.9 |
| 72512 | 9.8 | 1.8 | 2.26 | 5.5 / 9.4 |

Table 3. The *rms* deviation and offset for $T_e$ in the OH discharges obtained in the simulations with the original (columns 1 - 3) and re-normalised (column 4) Bohm-gyroBohm model under various assumptions. Estimations are performed for the time interval starting from 3 s and lasting till the first sawtooth crash or till the end of the current ramp up in the sawtooth-free plasmas. The estimations performed for the whole ramp up phase starting from 3 s are marked by (*).

| Shot # | rms / offset, % (peaked $Z_{eff}$, flat $P_{rad}$) | rms / offset, %. (peaked $Z_{eff}$, peaked $P_{rad}$) | rms / offset, % (flat $Z_{eff}$, peaked $P_{rad}$) | rms / offset, % (peaked $Z_{eff}$, flat $P_{rad}$, $C_{e,BgB} = 3.3$) |
|---|---|---|---|---|
| 72460 | 21.6 / -20.9 | 17.1 / -16.1 | 19.4 / -18.8 | 9.27 / 7.42 |
| 72464 | 32.3 / -31.2 | 27.3 / -26.3 | 29.7 / -28.2 | 7.23 / -1.73 |
| 72467 | 31.2 / -31<br>34.5 / -33.5* | 27.7 / -26.7<br>30.6 / -29.5* | 30 / -28.2<br>35.1 / -33* | 5.03 / 1.2<br>5.64 / -0.5* |
| 72504 | 40.3 / -39<br>42.5 / -41* | 36 / -34.9<br>38.4 / 37.2* | 34.2 / -32.6<br>39.7 / -37.5* | 8.73 / -5.75<br>10.7 / -7.8* |
| 72723 | 26.4 / -25.3 | 24 / -23 | 24 / -22.2 | 4.86 / 1.07 |

| | | | | |
|---|---|---|---|---|
| | 30.5 / -28.6* | 27.8 / -26* | 29.3 / -26.7* | 7.23 / -2.47* |
| 72465 | 40.2 / -39<br>46 / -44.9 | 36.3 / -34.8<br>42.3 / -41.6* | 38.4 / -36.2<br>45.3 / -43.7 | 7.1 / -2.8<br>11.4 / -8.5* |

Table 4 The *rms* deviation and offset for $T_e$ in the OH discharges obtained in simulations with the original (first and second columns) and re-normalised (third column) Coppi-Tang model. Estimations are performed for the sawtooth-free phase starting from 3 s.

| Shot # | rms / offset, % (peaked $Z_{eff}$, flat $P_{rad}$) | rms / offset, %. (peaked $Z_{eff}$, peaked $P_{rad}$) | rms / offset, % (peaked $Z_{eff}$, flat $P_{rad}$, $C_{e,CT} = 8$) |
|---|---|---|---|
| 72460 | 74 / -73 | 58 / -54 | 20.7 / 17.6 |
| 72464 | 92 / -90 | 72 / -67 | 14.5 / -4.2 |
| 72467 | 109 / -107 | 89 / -84 | 14.4 / -5.6 |
| 72504 | 115 / -112 | 97 / -93 | 18.1 / -12 |
| 72723 | 70 / -65 | 58 / -53 | 31.2 / -28 |
| 72465 | 130 / -126 | 111 / -106 | 18.3 / -11.8 |

Table 5. The *rms* deviation and offset for $T_e$ in the ICRF heated discharges obtained with empirical models under assumptions of peaked $Z_{eff}$ profile, $T_i/T_e$ ratio matching the measured neutron yield and Abel inverted radiative power profile. The time interval 5.5 - 7.4 s limited by the stable ICRF coupling and the absence of the sawteeth in #72507 (the low-amplitude sawtooth oscillations are observed in #72505) is used for estimations.

| Shot # | Original Bohm-gyroBohm model rms / offset, % | Re-normalised Bohm-gyroBohm model ($C_{e,BgB} = 3.3$) rms / offset, % | Re-normalised Coppi-Tang model ($C_{e,CT} = 4.9$) rms / offset, % |
|---|---|---|---|
| 72505 | 35.81 / -34.5 | 6.55 / 2.98 | 6.8 / 0.25 |
| 72507 | 11.58 / -3.77 | 25.91 / 24.86 | 22.3 / 19.6 |

Table 6. The *rms* deviation and offset for $T_e$ and $T_i$ in the NBI heated discharges obtained in simulations with the Bohm-gyroBohm, re-normalised Coppi-Tang ($C_{i,CT} = 8$, $C_{e,CT} = 4.7$) and GLF23 models. The estimations have been performed for the time interval starting from 3.5 s and lasting till the first sawtooth crash (6.5 s) in #72516, the end of the *L*-mode (7 s) in #72511 and formation of a steep ITB-like $T_i$ profile (4.8 s) in #72512.

| Shot # | Bohm-gyroBohm model rms / offset for $T_e$, % | Bohm-gyroBohm model rms / offset for $T_i$, % | Re normalised Coppi-Tang model rms / offset for $T_e$, % | Re normalised Coppi-Tang model rms / offset for $T_i$, % | GLF23 model rms / offset for $T_e$, % | GLF23 model rms / offset for $T_i$, % |
|---|---|---|---|---|---|---|
| 72516 | 8.46 /-5.96 | 7.4 / -0.88 | 8.95/1.22 | 8.05/3.36 | 9.78 / 8.54 | 6 / -2.96 |
| 72511 | 7.29 / 3.46 | 7.75 / -3.31 | 7.78/3.45 | 12.05/-0.65 | 23.2 / 19.9 | 17.2 / -11.3 |
| 72512 | 14.59/12.68 | 8.05 / 2.05 | 6.2 / 0.22 | 12.58/-7.23 | 23.6 / 21.6 | 28.17/-20.4 |

Figure captions

Fig. 1. Ohmic current ramp up discharges performed at different current ramp rate: plasma current (top), central line averaged density measured with the Thomson scattering diagnostics (middle) and electron temperature measured with the ECE diagnostics at 3 and at 3.5 m (bottom). Red, black and blue curves and symbols correspond to discharges 72464, 72467 and 72465 respectively.

Fig. 2. ICRF heated and reference OH discharges: ICRF power and plasma current (top), line averaged density measured with the Thomson scattering diagnostics (middle) and electron temperature measured with ECE diagnostics at 3m (bottom). Red, black and blue curves and symbols correspond to discharges 72505, 72467 and 72507 respectively.

Fig. 3. NBI assisted current ramp up: NBI power and plasma current (top), central line averaged density measured with the Thomson scattering diagnostics (middle), electron temperature measured with the ECE diagnostics at 3m (bottom, symbols) and ion temperature measured with the CX diagnostics at 3.05 m (bottom, curves). Black, blue and red curves and symbols correspond to discharges 72516, 72511 and 72512 respectively.

Fig. 4. (Top) Evolution of central safety factor obtained in TRANSP simulations with the ECE (red solid curve) and Thomson scattering (red dashed curve) data for electron temperature and flat $Z_{eff}$ profile. Blue curves show the $q_0$ obtained in ASTRA simulations performed with flat (solid curve) and peaked (dashed curve) $Z_{eff}$ profile using the ECE data for $T_e$. (Middle) Peaked and flat $Z_{eff}$ profiles used in simulations shown on the top panel. (Bottom) Electron (bold curve) and deuterium ion density

profile obtained at the end of the current ramp up using peaked (thin solid curve) and flat (dashed curve) $Z_{eff}$ profiles shown in the middle panel.

Fig. 5. Neutron yield simulated with TRANSP under different assumptions on $T_i$ and $Z_{eff}$: $T_i = T_e$ and flat $Z_{eff}$ (red solid curve), $T_i = T_e$ and peaked $Z_{eff}$ making the $q_0$ evolution consistent with the time of the first sawtooth crash (red dashed curve) and peaked $Z_{eff}$ and adjusted $T_i$ matching the measured neutron yield (blue curve). Black curve shows the measured neutron yield.

Fig. 6. $Z_{eff}$ profiles measured with the CX diagnostics in the middle and at the end of the current ramp up in the NBI heated discharges.

Fig. 7. Measured electron temperature (top) and simulated current density (middle) and safety factor (bottom) profiles in discharge with fast (red) and slow (blue) current ramp up. The ECE data for electron temperature mapped to the magnetic surfaces computed by TRANSP are shown. The profiles are shown at 3 (dashed curves), 4 (solid curves) and 5.2 s (dotted-dashed curves).

Fig. 8. Evolution of the safety factor in # 72507 simulated with the off-axis $Z_{eff}$ profiles making the $q_0$ evolution consistent with the time of the first sawtooth crash. Profiles are shown at 3 (solid curve), 4.1 (dashed curve), 6 (termination of the phase with Alfven cascades, dashed-dotted curve) and 7.4 s (before the first sawtooth crash, dotted curve).

Fig. 9. Electron temperature profiles simulated with the original and re-normalised by factor 3.3 Bohm-gyroBohm model (dashed and solid curves correspondingly) and profiles measured with the ECE (closed symbols) and Thomson scattering (open symbols with error bars) diagnostics for discharge with fast (top) and slow (bottom)

current ramp up. The profiles measured with the Thomson scattering diagnostics are averaged over 0.75 s. The measured $T_e$ profiles are mapped to the magnetic surfaces computed by ASTRA.

Fig. 10 Electron temperature obtained in the simulations with the original (dashed curves) and re-normalised by factor 8 (solid curves) Coppi-Tang model at 3 (black curves) and 6 (red curves) s for discharge 72464. Symbols show the measured (ECE) profiles mapped to the magnetic surfaces computed by ASTRA.

Fig. 11. Electron (solid curves) and ion (dashed curves) ICRF heating profiles at 7.5 s for #72505 (red curves) and 72507 (blue curves) simulated by TORIC in TRANSP using the adjusted $Z_{eff}$ profile and $T_i/T_e$ ratio. The heating profiles are averaged over 1 s.

Fig. 12. Electron temperature obtained in simulations with the original (red solid curves) and re-normalised ($C_{e,BgB}$ = 3.3, red dashed curves) Bohm-gyroBohm model, and with re-normalised Coppi-Tang model ($C_{e,CT}$ = 4.9, blue curves) for ICRF heated discharges 72505 (top) and 72507 (bottom) at 7 s. Symbols show the measured (ECE) profiles mapped to the magnetic surfaces computed by ASTRA.

Fig. 13. Electron (dashed curves) and ion (solid curves) beam power density in discharge 72516 (red) and 72511 (blue) at 6.5 s. Profiles are averaged over 0.4 s.

Fig. 14. Electron (left panels) and ion (right panels) temperature profiles simulated with the original Bohm-gyroBohm (red curves), GLF23 (green curves) and re-scaled Coppi-Tang ($C_{e,CT}$ = 4.7, $C_{i,CT}$ = 8, blue curves) model for discharges 72516 (top) and 72511 (bottom). Closed and open symbols with error bars on the left panels show the

measured (ECE and Thomson scattering correspondingly) $T_e$ profiles. Symbols on the right panels show the measured (CX) $T_i$ profiles. The error bars for the $T_i$ measurements are typically within 2%. All measured temperature profiles are mapped to the magnetic surfaces computed by ASTRA.

Fig. 15. ITER scenario: plasma current (black curve), minor radius (red curve), elongation (blue solid curve) and triangularity (blues dashed curve).

Fig. 16. Time of $q_0$ = 1 (top) and central electron (closed symbols) and ion (open symbols) temperature achieved at the end of the current ramp up (middle) in simulations with the GLF23 (red symbols) and original Bohm-gyroBohm (black symbols) model. Bottom panel shows the temperature profiles obtained at the beginning of the heating power plateau (7 s, solid curves) and at the end of the current ramp up (80 s, dashed curves) in simulations with 4 MW of auxiliary electron heating power using the GLF23 (red curves) and Bohm-gyroBohm (black curves) model.

Fig. 17. Evolution of the $q_0$ in OH and auxiliary heated plasmas with various heating powers (top) and current density profiles at 12 s (bottom left) and 80 s (bottom right). Solid, dotted-dashed and dashed curves show the results obtained in simulations with 0 (Ohmic plasma), 4 and 16 MW of heating power correspondingly.

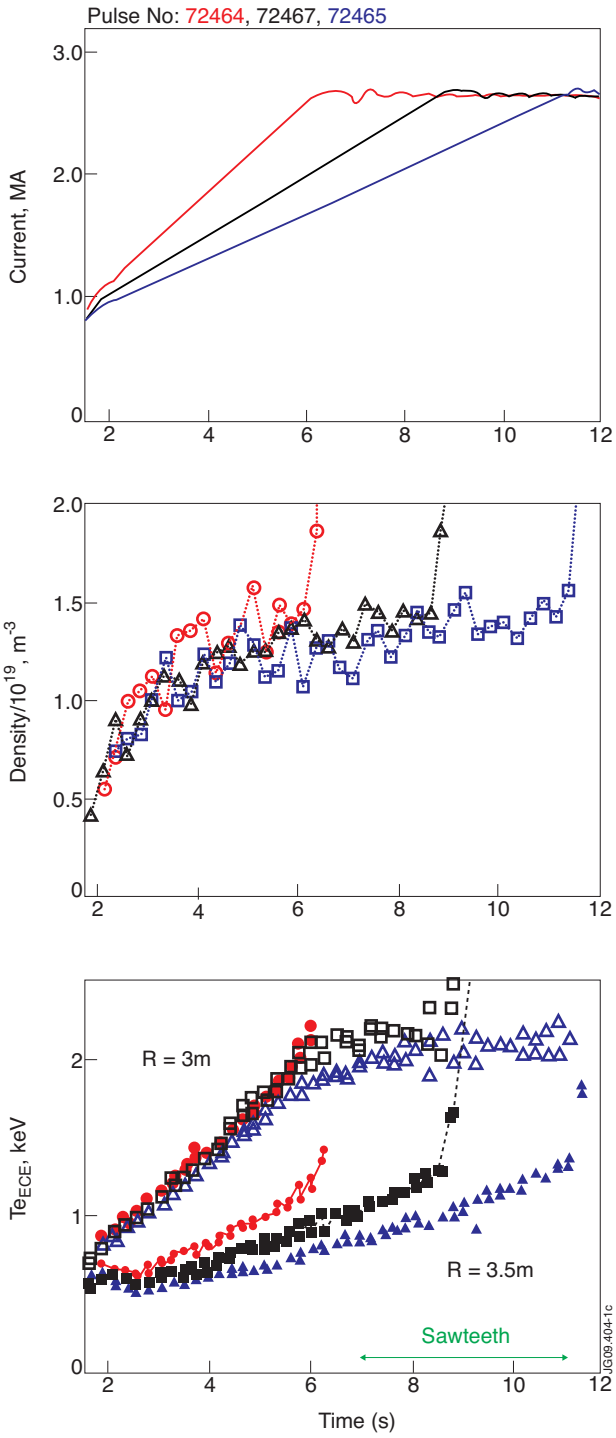
Pulse No: 72464, 72467, 72465
Current, MA
Density/10^19, m^-3
Te_ECE, keV
R = 3m
R = 3.5m
Sawteeth
Time (s)
JG09.404-1c

Figure 1

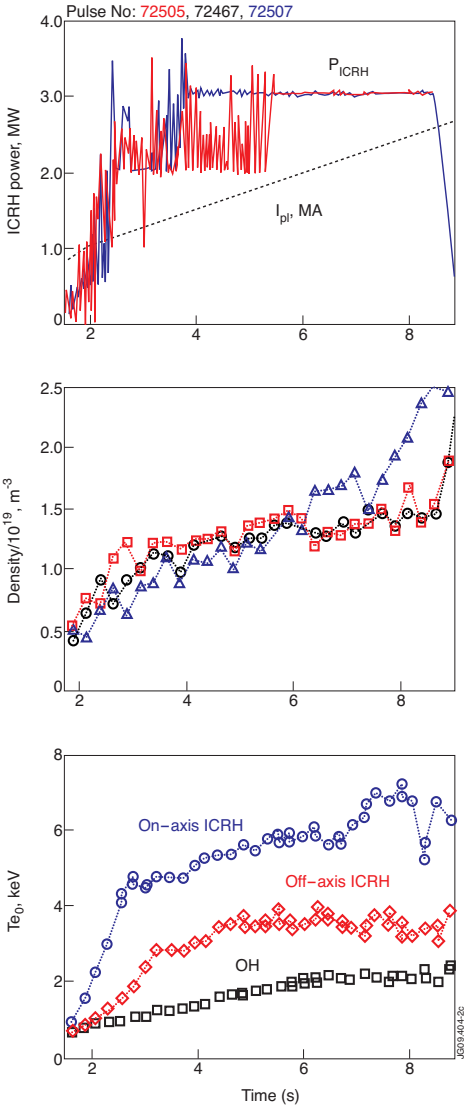
Pulse No: 72505, 72467, 72507
ICRH power, MW
P_ICRH
I_pl, MA
Density/10^19, m^-3
Te_0, keV
On−axis ICRH
Off−axis ICRH
OH
Time (s)

Figure 2

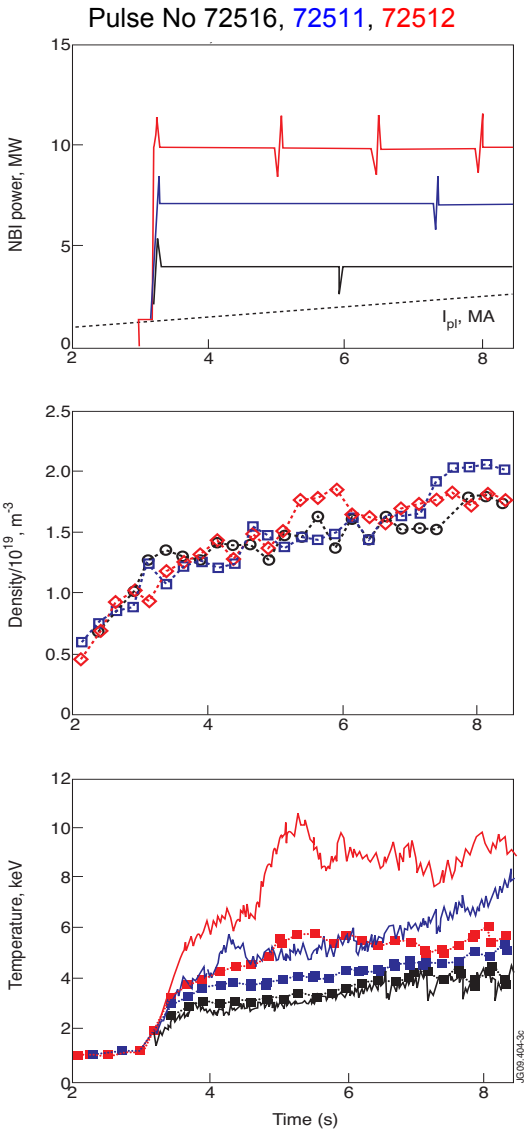
Pulse No 72516, 72511, 72512
NBI power, MW
$I_{pl}$, MA
Density/$10^{19}$, $m^{-3}$
Temperature, keV
Time (s)
J6309.404-3c

Figure 3

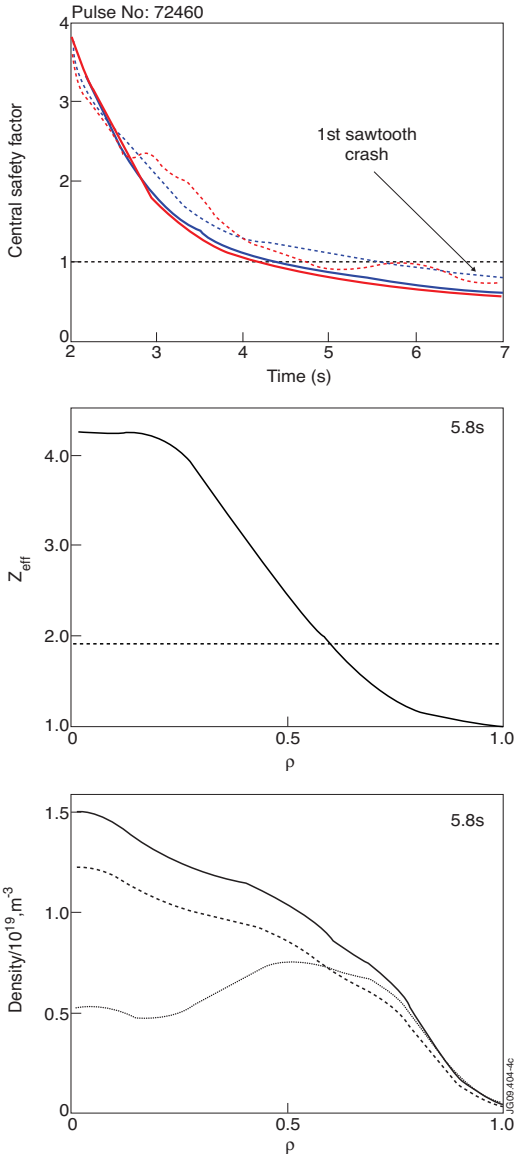
Pulse No: 72460
Central safety factor
1st sawtooth
crash
Time (s)
5.8s
$Z_{eff}$
ρ
5.8s
Density/$10^{19}$,$m^{-3}$
ρ
JG08.404-4c

Figure 4

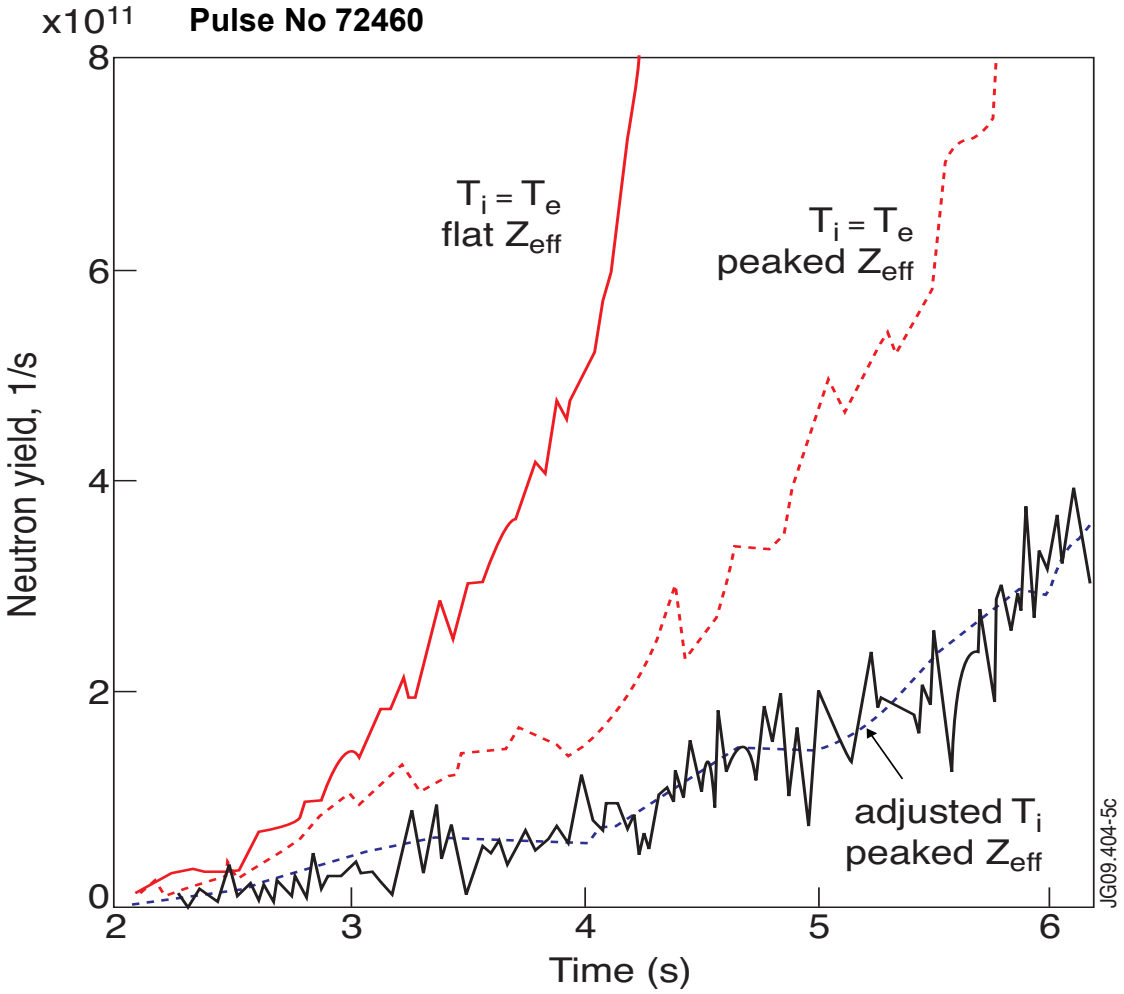
x10^11
Pulse No 72460
Neutron yield, 1/s
Time (s)
T_i = T_e
flat Z_eff
T_i = T_e
peaked Z_eff
adjusted T_i
peaked Z_eff
JG09.404-5c

Figure 5

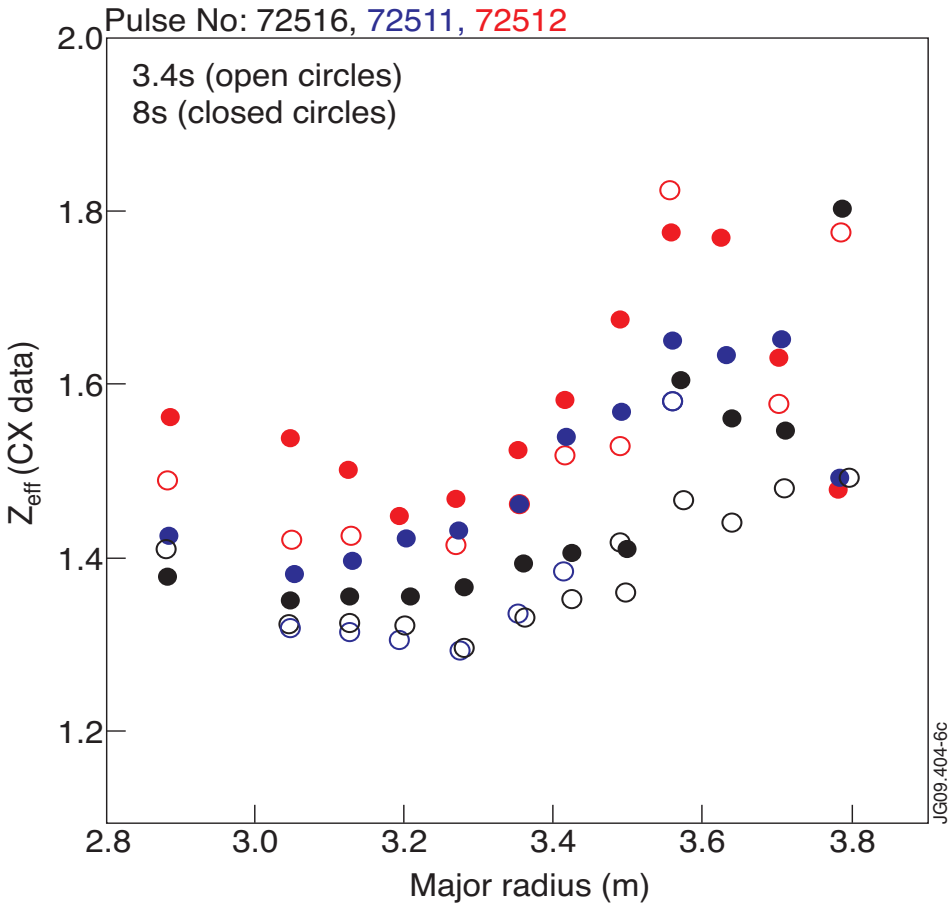
Pulse No: 72516, 72511, 72512
3.4s (open circles)
8s (closed circles)
$Z_{eff}$ (CX data)
2.0
1.8
1.6
1.4
1.2
2.8
3.0
3.2
3.4
3.6
3.8
Major radius (m)
JG09.404-6c

Figure 6

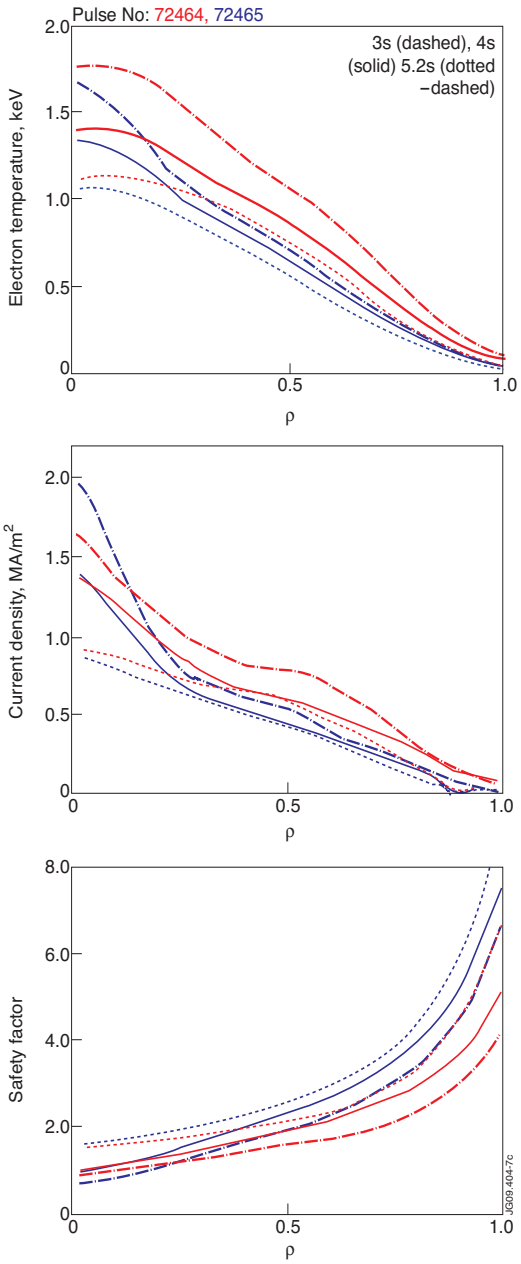
Pulse No: 72464, 72465
3s (dashed), 4s
(solid) 5.2s (dotted
–dashed)
Electron temperature, keV
Current density, MA/m2
Safety factor
ρ
IG09.404-7c

Figure 7

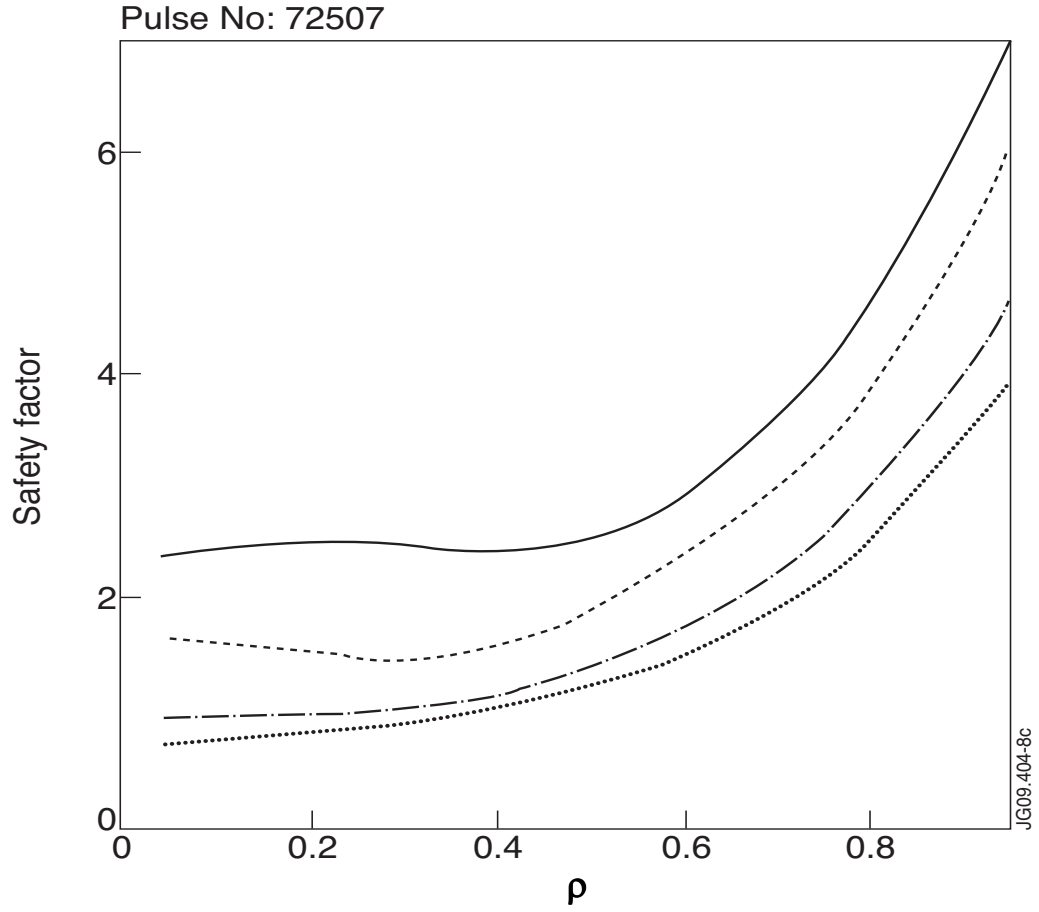


Figure 8

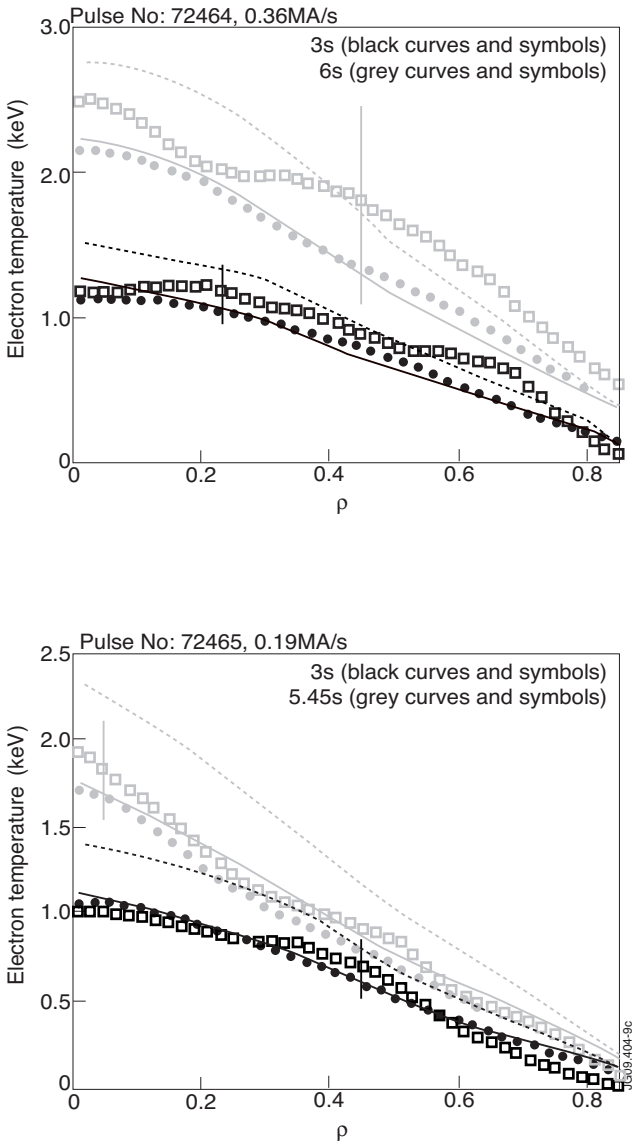
Pulse No: 72464, 0.36MA/s
3s (black curves and symbols)
6s (grey curves and symbols)
Electron temperature (keV)
3.0
2.0
1.0
0
0
0.2
0.4
0.6
0.8
ρ
Pulse No: 72465, 0.19MA/s
3s (black curves and symbols)
5.45s (grey curves and symbols)
Electron temperature (keV)
2.5
2.0
1.5
1.0
0.5
0
0
0.2
0.4
0.6
0.8
ρ

Figure 9

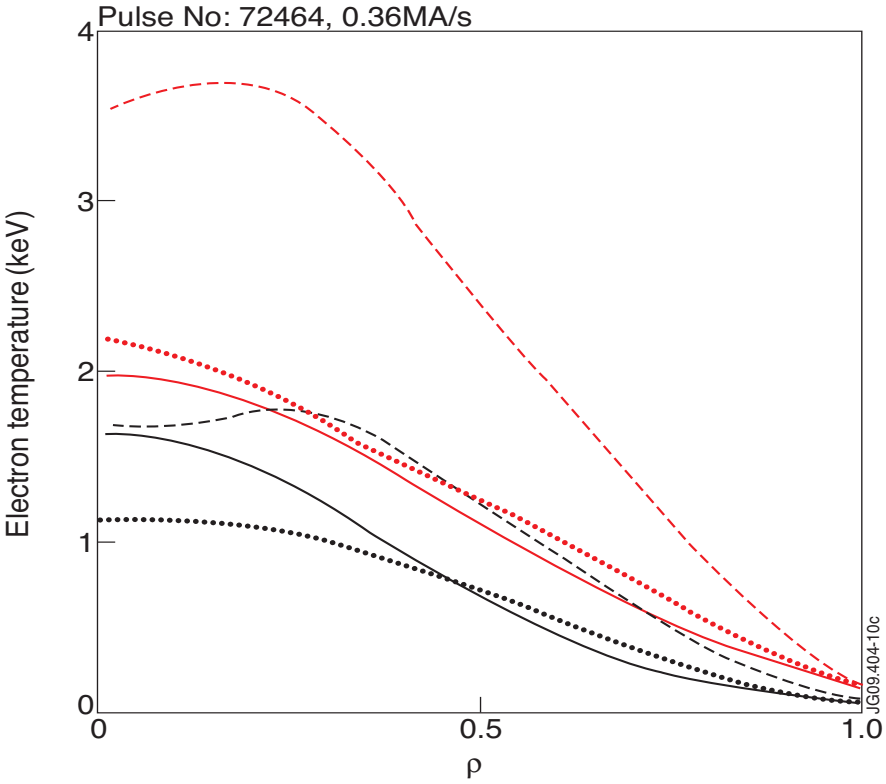
Pulse No: 72464, 0.36MA/s
Electron temperature (keV)
4
3
2
1
0
0
0.5
1.0
ρ
JG09.404-10c

Figure 10

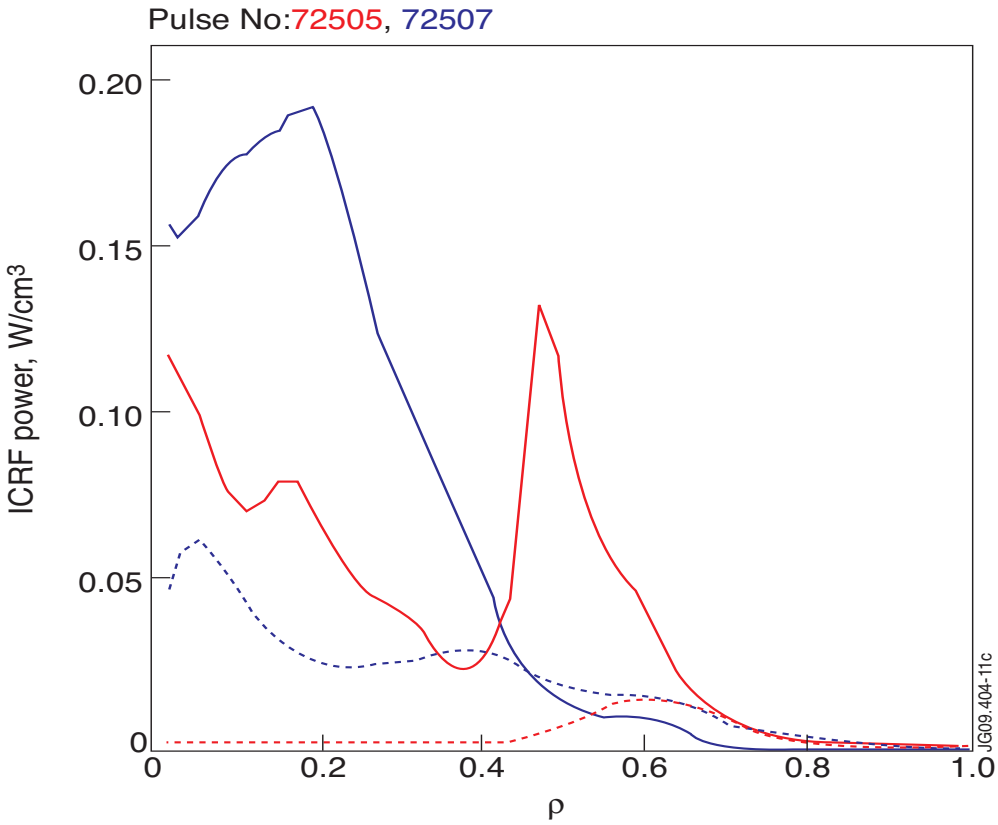
Pulse No:72505, 72507
ICRF power, W/cm3
0.20
0.15
0.10
0.05
0
0
0.2
0.4
0.6
0.8
1.0
ρ
JG09.404-11c

Figure 11

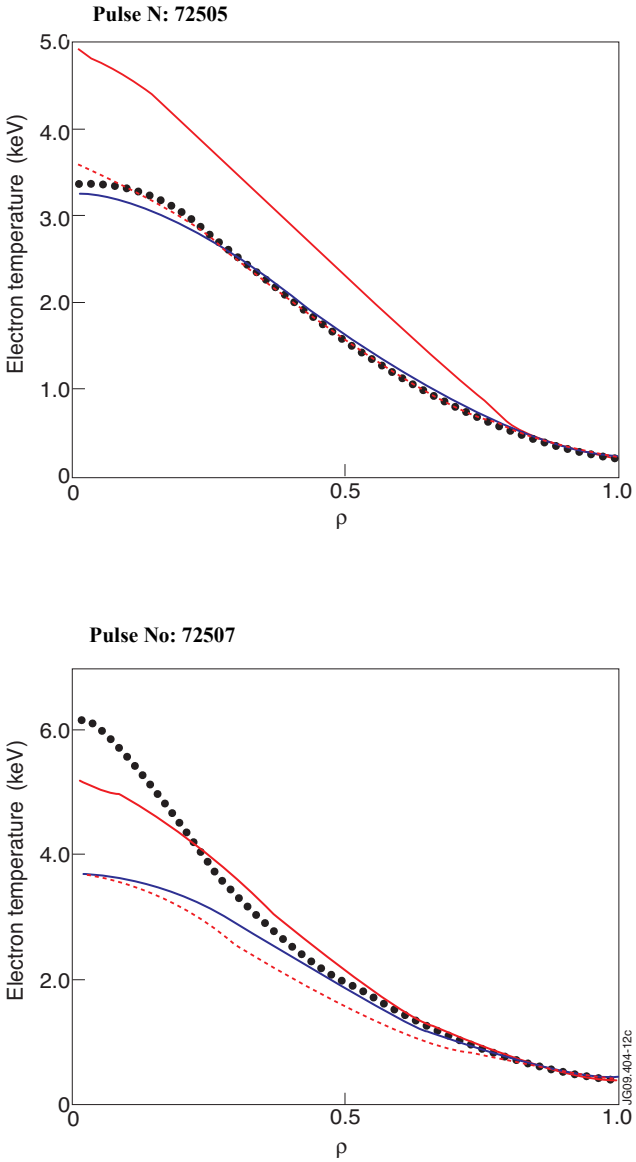
Pulse N: 72505
Electron temperature (keV)
5.0
4.0
3.0
2.0
1.0
0
0
0.5
1.0
ρ
Pulse No: 72507
Electron temperature (keV)
6.0
4.0
2.0
0
0
0.5
1.0
ρ
JG09.404-12c

Figure 12

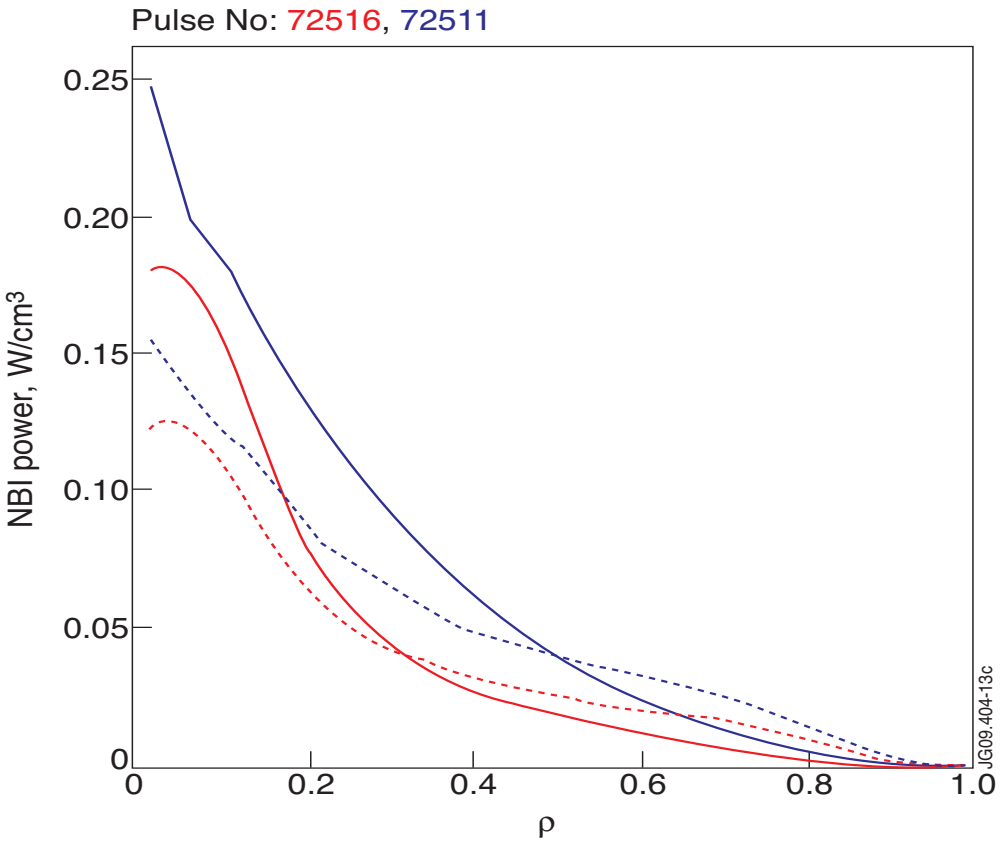
Pulse No: 72516, 72511
NBI power, W/cm3
0.25
0.20
0.15
0.10
0.05
0
0
0.2
0.4
0.6
0.8
1.0
ρ
JG09.404-13c

Figure 13

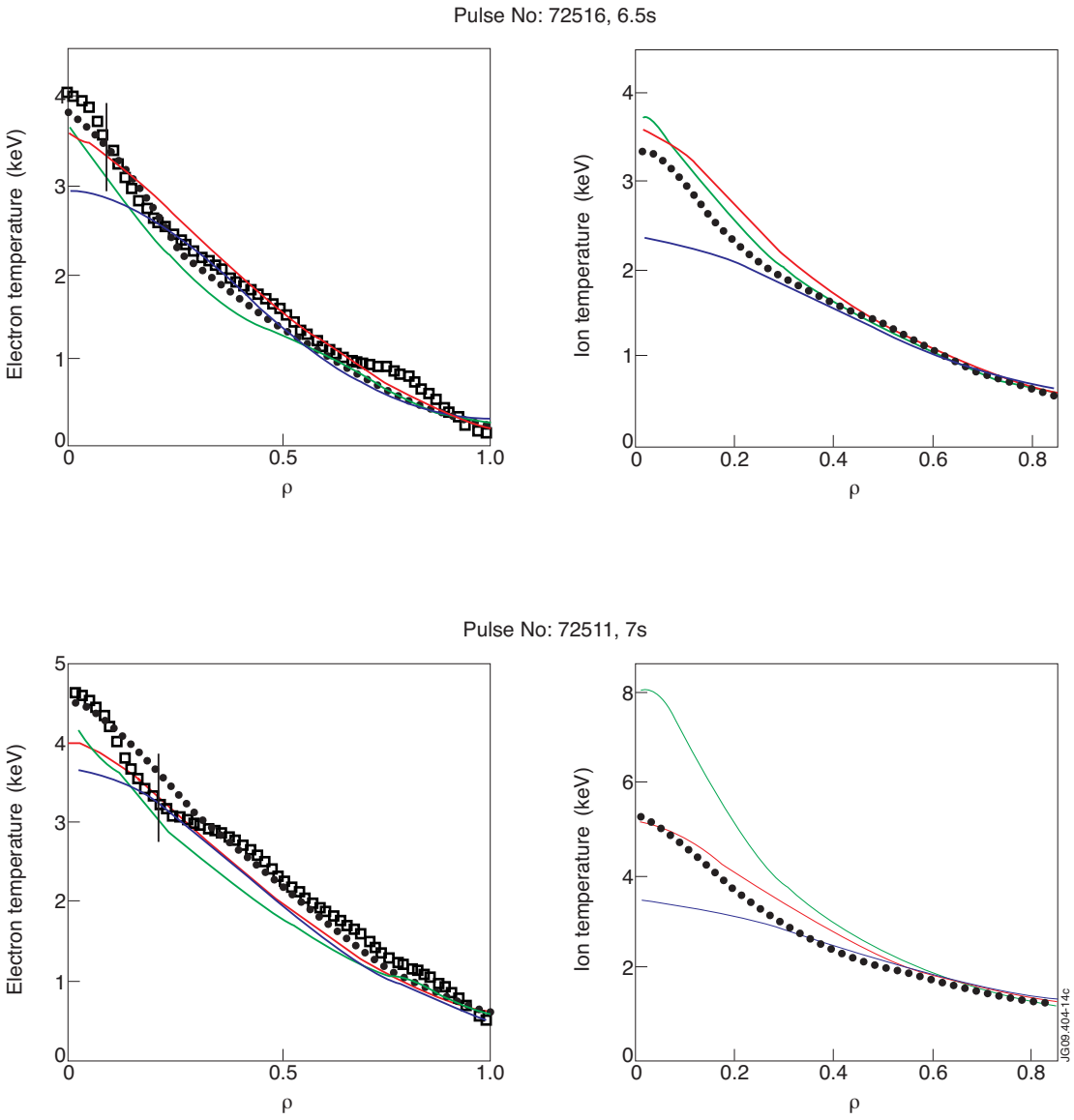
Pulse No: 72516, 6.5s
Electron temperature (keV)
Ion temperature (keV)
ρ
ρ
Pulse No: 72511, 7s
Electron temperature (keV)
Ion temperature (keV)
ρ
ρ
JG09.404-14c

Figure 14

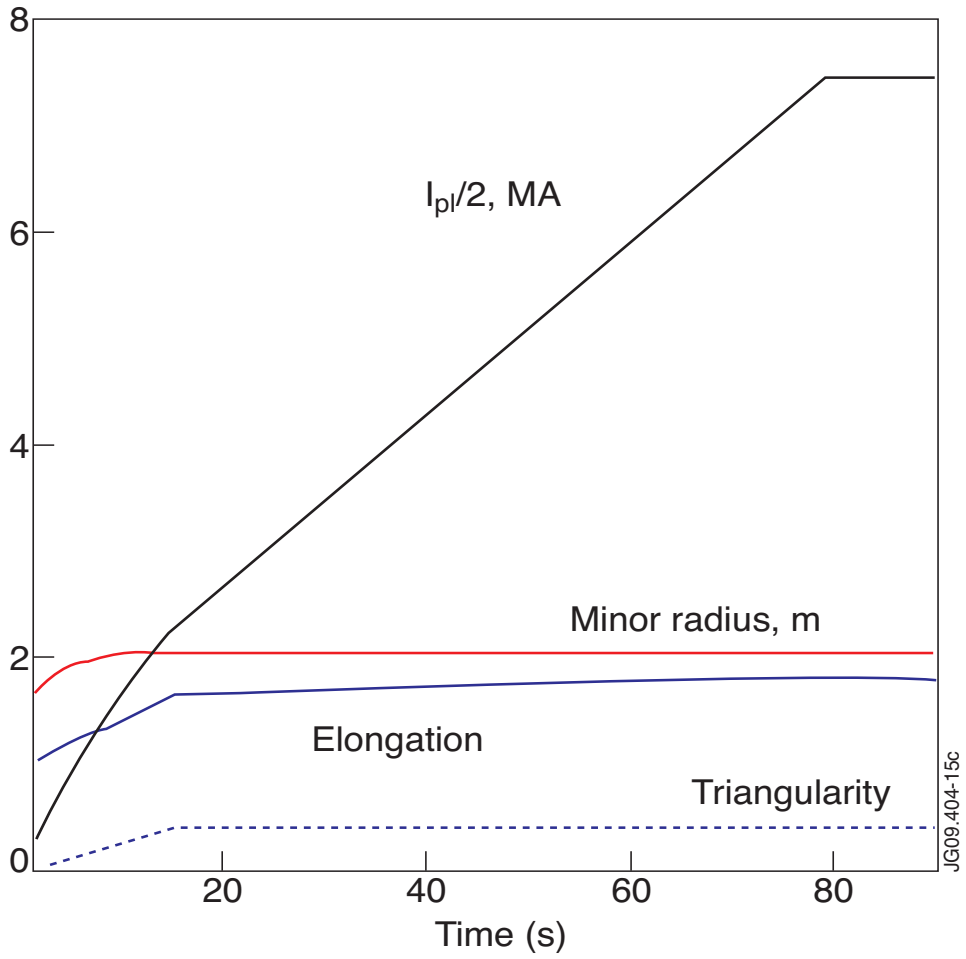
8
6
4
2
0
$I_{pl}$/2, MA
Minor radius, m
Elongation
Triangularity
20
40
60
80
Time (s)
JG09.404-15c

Figure 15

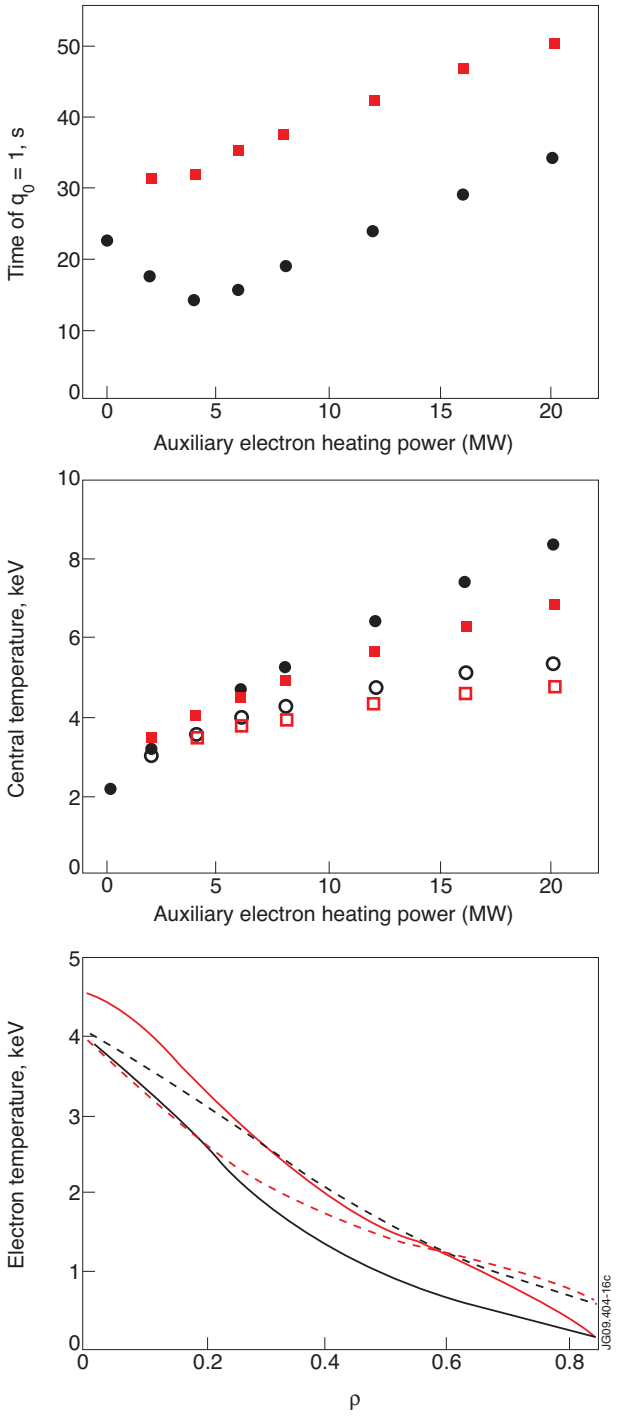
Time of $q_0$ = 1, s
Auxiliary electron heating power (MW)
Central temperature, keV
Auxiliary electron heating power (MW)
Electron temperature, keV
ρ
JG09.404-16c

Figure 16

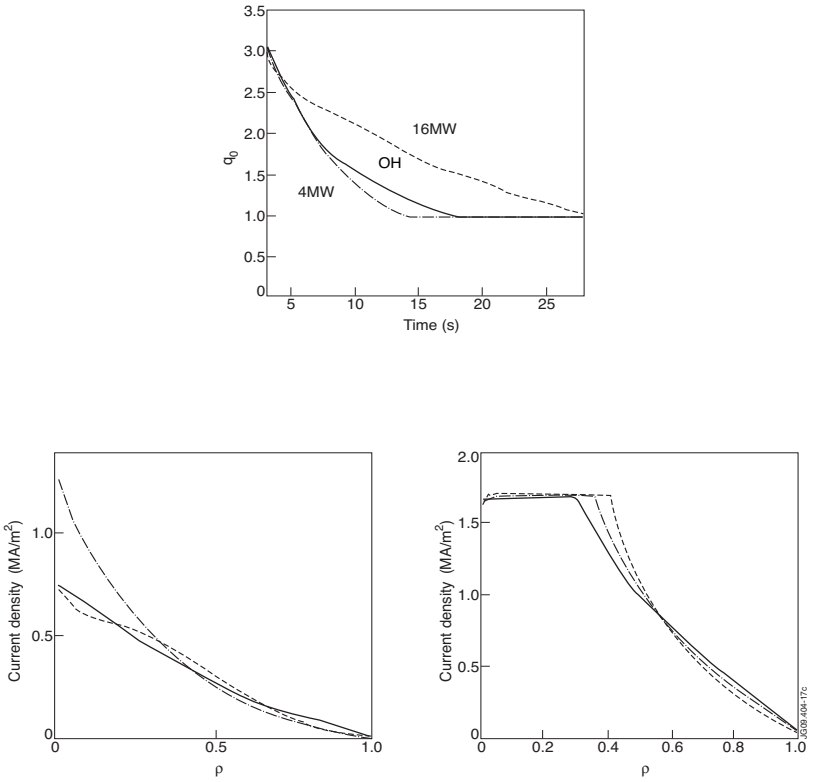
3.5
3.0
2.5
2.0
1.5
1.0
0.5
0
$q_0$
16MW
OH
4MW
5
10
15
20
25
Time (s)
Current density (MA/m$^2$)
1.0
0.5
0
0
0.5
1.0
ρ
Current density (MA/m$^2$)
2.0
1.5
1.0
0.5
0
0
0.2
0.4
0.6
0.8
1.0
ρ
JG09.404-17c

Figure 17